Provided for non-commercial research and education use.
Not for reproduction, distribution or commercial use.

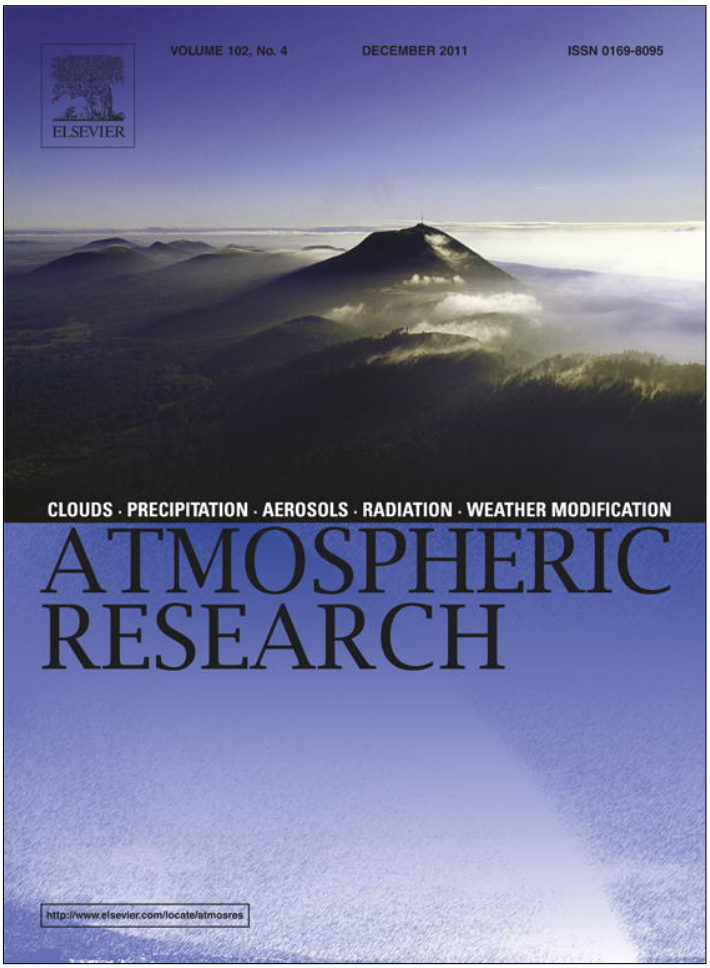

This article appeared in a journal published by Elsevier. The attached copy is furnished to the author for internal non-commercial research and education use, including for instruction at the authors institution and sharing with colleagues.

Other uses, including reproduction and distribution, or selling or licensing copies, or posting to personal, institutional or third party websites are prohibited.

In most cases authors are permitted to post their version of the article (e.g. in Word or Tex form) to their personal website or institutional repository. Authors requiring further information regarding Elsevier's archiving and manuscript policies are encouraged to visit:

http://www.elsevier.com/copyright

Author's personal copy

Atmospheric Research 102 (2011) 365–393

Contents lists available at SciVerse ScienceDirect

Atmospheric Research

journal homepage: www.elsevier.com/locate/atmos

Climatology of aerosol radiative properties in the free troposphere

E. Andrews [a,b,*], J.A. Ogren [a], P. Bonasoni [c], A. Marinoni [c], E. Cuevas [d], S. Rodríguez [d], J.Y. Sun [e], D.A. Jaffe [f], E.V. Fischer [g,1], U. Baltensperger [h], E. Weingartner [h], M. Collaud Coen [i], S. Sharma [j], A.M. Macdonald [j], W.R. Leaitch [j], N.-H. Lin [k], P. Laj [l], T. Arsov [m], I. Kalapov [m], A. Jefferson [a,b], P. Sheridan [a]

[a] National Oceanic and Atmospheric Administration, Earth Systems Research Laboratory, Boulder, CO 80305, USA
[b] University of Colorado, CIRES, Boulder, CO 80305, USA
[c] ISAC-CNR, Institute of Atmospheric Sciences and Climate, Bologna I-40129, Italy
[d] Izaña Atmospheric Research Centre, AEMET, Joint Research Unit with CSIC "Studies on Atmospheric Pollution", 38071, Santa Cruz de Tenerife, Canary Islands, Spain
[e] Key Laboratory for Atmospheric Chemistry, Chinese Academy of Meteorological Sciences, Beijing 100081, China
[f] University of Washington, Department of Atmospheric Sciences, Seattle, WA 98195, USA
[g] Harvard University, School of Engineering and Applied Sciences, Cambridge, MA 02138, USA
[h] Paul Scherrer Institut, Laboratory of Atmospheric Chemistry, Villigen PSI, CH-5232, Switzerland
[i] Federal Office of Meteorology and Climatology, MeteoSwiss, CH-1530 Payerne, Switzerland
[j] Environment Canada, Toronto, Ontario, M3H 5T4, Canada
[k] Department of Atmospheric Sciences, National Central University, Chung-Li 320, Taiwan
[l] UJF-Grenoble 1/CNRS, LGGE UMR 5183, Grenoble, F-38041, France
[m] Institute for Nuclear Research and Nuclear Energy, Sofia BG-1784, Bulgaria

ARTICLE INFO

Article history:
Received 2 February 2011
Received in revised form 25 August 2011
Accepted 29 August 2011

Keywords:
Aerosol radiative properties
Free troposphere
Climatology

ABSTRACT

High altitude mountaintop observatories provide the opportunity to study aerosol properties in the free troposphere without the added expense and difficulty of making airborne measurements. Climatologies for free tropospheric aerosol radiative properties in cloud-free air, including light scattering, light absorption, light extinction, single scattering albedo, Ångström exponent, hemispheric backscatter fraction and radiative forcing efficiency, from twelve high altitude (2.2–5.1 km) measurement platforms are presented at low relative humidity and at standard temperature and pressure. These climatologies utilize data from ten mountaintop observatories in the 20–50ºN latitude band: Mauna Loa, USA; Lulin Mountain, Taiwan; Nepal Climate Observatory — Pyramid; Izaña, Spain; Mount Waliguan, China; Beo Moussala, Bulgaria; Mount Bachelor, USA; Monte Cimone, Italy; Jungfraujoch, Switzerland; Whistler Mountain, Canada. Results are also included from two multi-year, in-situ aerosol vertical profiling programs: Southern Great Plains, USA and Bondville, USA. The amount of light absorption and scattering observed at these high altitude sites either peaks in the spring or it has a broad spring to summer enhancement. The seasonal variation of the aerosol single scattering albedo, backscatter fraction and Ångström exponent changes from site to site but the timing can be related to aerosol sources and transport processes known to impact the individual sites. The seasonal variation of in-situ aerosol light extinction from these high altitude measurements is in excellent agreement with extinction values derived from CALIPSO lidar measurements. Analysis of the systematic variability among in-situ aerosol properties shows that these relationships can be used to infer aerosol types. In particular, the relationship between single scattering albedo and Ångström exponent can indicate the presence of dust aerosol. Radiative forcing efficiency (RFE = aerosol forcing/aerosol optical depth) is used to

* Corresponding author at: National Oceanic and Atmospheric Administration, Earth Systems Research Laboratory, Boulder, CO 80305, USA.
E-mail address: betsy.andrews@noaa.gov (E. Andrews).
[1] E. Fischer performed this work while at University of Washington, Department of Atmospheric Sciences, Seattle, 98195, Washington, USA.

0169-8095/$ – see front matter © 2011 Elsevier B.V. All rights reserved.
doi:10.1016/j.atmosres.2011.08.017

Author's personal copy

assess the importance of single scattering albedo and backscatter fraction on aerosol forcing by eliminating aerosol amount (i.e., aerosol optical depth) from the calculation. Variability in monthly cycles of RFE corresponds with changes in single scattering albedo and hemispheric backscatter fraction. Utilizing site-specific, climatological values of single scattering albedo and backscatter fraction to calculate RFE results in departures from the monthly median values of RFE typically in the range 10–30%. The greatest discrepancy occurs for months with low aerosol loading where the observed variability of single scattering albedo and backscatter fraction is the greatest. At most sites the radiative forcing efficiency at low aerosol loading (light scattering $<10\ Mm^{-1}$) is slightly less negative (more warming) than at higher aerosol loading.

© 2011 Elsevier B.V. All rights reserved.

Contents

1. Introduction

Atmospheric aerosol particles affect the earth's radiative balance in several ways. They can scatter and absorb radiation, directly changing how much radiation reaches any particular location. Furthermore, aerosol particles indirectly influence the earth's radiative balance by acting as cloud nuclei. The magnitude and sign of the aerosol forcing effect are determined, in part, by both the horizontal and vertical distribution of the aerosol particles (Haywood and Ramaswamy, 1998). The horizontal distribution of aerosol particles is important because the aerosol forcing changes with the underlying surface (e.g., ocean, snow, etc.) as well as the solar angle and length of day. The vertical location of atmospheric particles on the other hand affects the thermal profile of the atmosphere. Sanroma et al. (2010) suggested that, during cloud-free conditions,

Author's personal copy

high altitude aerosol particles are the major contributor to variations in solar radiation flux reaching the surface, at least at the high altitude sites they studied. The positive radiative forcing associated with strongly absorbing particles is amplified when these particles are located above clouds (Zarzycki and Bond, 2010 and references within).

With lifetimes on the order of days to weeks, aerosols are not distributed homogeneously in the atmosphere. This results in local, regional and global differences in radiative forcing and creates an observational challenge. Near the surface, the coverage of geographic or global variation in aerosol properties due different mixes of aerosol sources and atmospheric processing is often addressed by using networks of measurement sites. Two examples are NOAA's baseline observatory network (http://www.esrl.noaa.gov/gmd/) which focuses on monitoring background air and the European Supersites for Atmospheric Aerosol Research (EUSAAR) network designed to investigate regional atmospheric properties in terms of air quality, climate change and long range transport (www.eusaar.net/). Vertical profiles and high altitude measurements of aerosol optical properties are sparse. During field campaigns instrumented airplanes may obtain a small number of profiles over a short period of time. While these short-term measurements provide valuable in-depth information about processes and events, campaign-based aircraft aerosol observations are not designed to diagnose the annual or seasonal climatology of aerosol optical properties. Additionally, due to the short-term nature of field campaigns, there is often little information about whether the results are representative of the region and/or time period. Surface and spaced-based lidars can provide long-term time series of aerosol backscattering, and sometimes extinction, as a function of altitude but they are do not measure key climate variables such as aerosol single scattering albedo or asymmetry parameter. High altitude mountaintop observatories provide the opportunity to make long-term, continuous observations of in-situ aerosol properties in the free troposphere (FT) without the added expense and difficulty of making airborne measurements. Diurnal and synoptic flow patterns can bring varying degrees of boundary-layer or FT air to mountaintop sites. Though segregating boundary layer and FT air can be a challenge, high altitude sites provide a unique opportunity to understand differences and similarities in aerosol properties between these two layers.

Aerosol transport in the free troposphere has important implications for both air quality and climate (Laj et al., 2009). Faster wind speeds in the FT allow aerosols that have been injected into this layer to be transported over long distances. Once lofted into the FT, dust, biomass burning smoke and anthropogenic pollution aerosols from surface sources can be transported hemispherically (e.g., McKendry et al., 2001; Wandinger et al., 2002; Mattis et al., 2008). Under favorable meteorological conditions, aerosols that have been redistributed in the FT can be entrained back down to the surface, affecting air quality thousands of kilometers from the aerosol source region (e.g., McKendry et al., 2001, Colette et al., 2008).

Laj et al. (2009) suggest that the FT is more spatially representative of the global atmosphere than the boundary layer because aerosol residence times in the FT can be on the order of several weeks (Kent et al., 1998). Thus aerosols that are transported through the FT may have extended climate and air quality impacts. This also implies that long-term measurements in the free troposphere may be more useful for satellite validation than those located close to surface aerosol sources. Most surface aerosol measurement sites are within the boundary layer, however there is a small subset of high elevation sites.

The existing literature on in-situ aerosol measurements falls into two categories. The first category encompasses detailed analyses of long-term aerosol optical property measurements for individual observatories. Some examples for the high altitude measurement platforms included here are: Marcq et al. (2010), Collaud Coen et al. (2007), Marinoni et al. (2008), Andrews et al. (2004), Nyeki et al. (1998a), and Bodhaine (1983). These in-depth analyses provide a wealth of information about the sources and transport of aerosols to the site, temporal cycles (diurnal to seasonal), etc., but the data are not presented to allow a direct comparison with observations from other locations. The second category compares long-term aerosol optical measurements from several sites. The goals of these studies are either to diagnose regional trends or to identify differences between observations due to location and predominant air mass types. Examples in this category include Delene and Ogren (2002), Gebhart et al. (2001), Bodhaine (1983), and Bodhaine (1995), however none of these studies focused on high altitude measurements. To our knowledge, this is the first paper comparing long-term in-situ aerosol optical measurements from high altitude observatories.

This work presents the first climatology of northern hemisphere (20–50°N) FT aerosol optical properties based on continuous, long-term in-situ measurements at high altitude observatories. By bringing together measurements from unrelated networks and sites we address knowledge gaps, such as those identified by Laj et al. (2009). Over the last several decades the number of mountaintop observatories continuously measuring in-situ aerosol radiative properties has increased significantly from a single station (Mauna Loa, USA) in the 1970s to at least ten observatories actively making these measurements today. By taking this data set as a whole and developing a self-consistent climatology, the combined observatory measurements of FT aerosol radiative properties have the potential to contribute to aerosol-climate research in a way that far exceeds the contribution from individual observatories. For example, this type of analysis may help constrain chemical transport models, validate satellite measurements, and quantify the influence of anthropogenic pollution, smoke, volcanoes and dust episodes on FT aerosol properties.

Using high altitude measurements, screened for both cloud contamination and boundary layer contamination (the screening is described below), the following questions are addressed:

(1) What are the similarities and differences in the means and variability of free-tropospheric aerosol radiative properties at a wide range of locations?
(2) How do these in-situ climatologies of free tropospheric light extinction compare to the satellite-derived climatologies?
(3) Do FT aerosol radiative properties vary systematically? What (if anything) does this systematic variation suggest about aerosol sources?
(4) What is the relative importance of aerosol amount and aerosol optical properties for direct radiative forcing calculations?

Author's personal copy

2. Methodology

2.1. Site descriptions

The aerosol climatology presented here utilizes in-situ data from ten mountaintop observatories in the 20–50ºN latitude band shown in Fig. 1 with site information (e.g., size cut, instrumentation, and length of data sets) listed in Table 1. Results are also included from two multi-year, in-situ aerosol vertical profiling programs performed using small instrumented aircraft: Southern Great Plains, USA (SGP) and Bondville, USA (BND). Sites were chosen based on the following criteria: (a) availability of long-term (>1 year) continuous measurements of light scattering and (except Beo Moussala (BEO)) light absorption and (b) station elevation sufficiently high (>2 km asl) to frequently sample FT air (note: the surrounding terrain will also play a role in determining whether a site is frequently in the FT, however a simple topographical parameterization is not, to our knowledge, something that can easily be determined on a site-by-site basis). Potential sites were initially identified using the GAWSIS database (http://gaw.empa.ch/gawsis/). The sites meeting these two criteria were all in the 20–50°N latitude range with the exception of South Pole (90.0°S, 2841 m asl) which was considered too clean/remote to be included here. Some additional information about each of the sites included in this study is described below. Note: where there is a difference, we have used the site ID tag in the GAW database rather than the local site acronym or identifier.

2.1.1. Mauna Loa, USA (MLO)

The Mauna Loa Observatory was established in 1956 on the island of Hawaii as a site for atmospheric and meteorological measurements. The National Oceanic and Atmospheric Administration (NOAA) Geophysical Monitoring for Climatic Change (GMCC) program (now the NOAA Earth System Research Laboratory (ESRL) Global Monitoring Division) began long-term monitoring of aerosol light scattering at MLO in 1974 and light absorption in 1990. Here, we only use data from 2001 onward as that is when the instruments consistent with those at the other sites in this study were installed. The current instrument installation at MLO is similar to that described in Sheridan et al. (2001). Bodhaine (1983) and Bodhaine (1995) present time series of the first eight years of light scattering and light absorption at MLO and note a strong seasonal cycle where higher scattering and absorption are observed in the springtime. These peaks were attributed to long-range transport of Asian dust and pollution (e.g., Perry et al., 1999).

2.1.2. Whistler, Canada (WHI)

The observatory at Whistler Mountain in British Columbia is operated by Environment Canada and has been collecting gas and aerosol data since March 2002 (Macdonald et al., 2011). Aerosol optical property measurements began in 2008. Physical and chemical measurements of the aerosol measured at WHI are described by Takahama et al. (2011). The measurements of aerosol radiative properties are discussed by McKendry et al. (2011). WHI is influenced by air masses conveyed across the Pacific from Asia (e.g., Leaitch et al., 2009; Macdonald et al., 2011) in the spring and Saharan dust can reach this site on occasion (McKendry et al., 2007). Biogenic aerosols are measured at the site during the late spring and summer and regional forest fires often influence the site during the mid to late summer (e.g. Takahama et al., 2011; McKendry et al., 2011). The site experiences FT air frequently during the fall to early spring with increasing boundary layer influence during late spring and into the summer (Gallagher et al., 2011; Macdonald et al., 2011).

2.1.3. Mount Bachelor, USA (MBO)

Mount Bachelor Observatory is situated on a dormant volcano in central Oregon. Mount Bachelor is home to a ski area, and the instruments are located in the summit lift building. The aerosol instrument set-up is described in Fischer et al. (2010). Analysis of springtime observations from MBO has shown that it is impacted by long range transport of Asian dust, pollution and biomass burning aerosols (Weiss-Penzias et al., 2007; Fischer et al., 2010). Some of the MBO aerosol instruments are only deployed in the springtime as a major focus of the observatory is trans-Pacific transport, so the annual cycle of light absorption and some intensive properties are not described here. This site differs from the others in this study in that a 1 μm aerodynamic impactor was deployed upstream of the aerosol instruments. Thus the MBO observations only represent sub-μm aerosols.

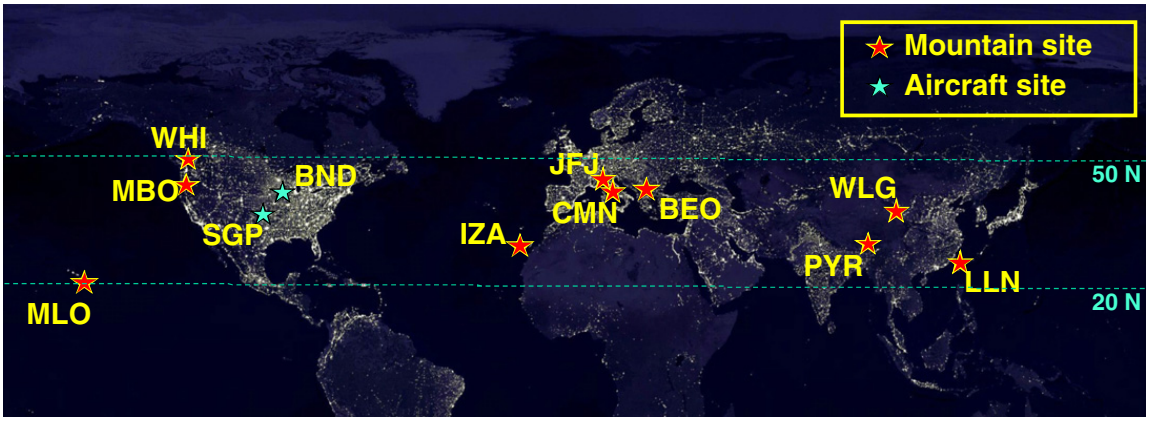

Fig. 1. Map of stations super-imposed on a NASA city lights image(http://visibleearth.nasa.gov/view_rec.php?id=1438).

Table 1
List of observatories included in this study, arranged from west to east.

Station	Lat/long elev (km) asl	Scat inst[a]	Abs inst[b]	Size cut (μm)	Years scat data	Years abs data	Contacts[c]	Network(s)[d]	Sample RH	RH>95%[e]
MLO Mauna Loa, USA	19.54 N 155.58 W 3.4	T	P	10	2000–2009	2000–2009	Ogren	NB, GAW	controlled <40%	7%
WHI Whistler, Canada	50.01 N 122.95 W 2.2	T	P	2.5	2008–2009	2008–2009	Leaitch, Macdonald	NC, EC, GAW	Typically <40%	23%
MBO Mt Bachelor, USA	43.98 N 121.70 W 2.8	T, R	P	1	April, May, 2008–2009 T 2005–2009 R	April, May 2008–2009	Jaffe	None	Typically <40%	47%
SGP[f] Southern Great Plains, USA	36.61 N 97.49 W 3–5	T	P	7	2000–2007	2000–2007	Ogren	NC	controlled <40%	–
BND[f] Bondville, USA	40.05 N 88.37 W 3–5	T	P	7	2006–2009	2006–2009	Ogren	NC	controlled <40%	–
IZA Izana, Spain	28.47 N 16.25 W 2.4	T	M	10	2008–2009	2008–2009	Cuevas, Rodríguez	GAW	Typically <40%	8%
JFJ Jungfraujoch, Switzerland	46.55 N 7.99E 3.6	T	A	Whole air	1995–2007	2001–2007	Baltensperger, Weingartner, Collaud Coen	EUSAAR, GAW	controlled <20%	38%
CMN Mt. Cimone, Italy	44.18 N 10.70E 2.2	E	P, M	Whole air	2007–2009	2007–2009	Bonasoni, Marinoni	EUSAAR, GAW	Typically <40%	34%
BEO Beo Moussala Bulgaria	42.18 N 23.59E 2.4	T	–	Whole air	2007–2009	2007–2009	Kalapov	NC, GAW	Typically <40%	–
PYR Pyramid, Nepal	27.57 N 86.48E 5.1	T	M	2.5 (σ_{sp}) 10 (σ_{ap})	2006–2008	2006–2008	Laj	GAW, ABC	controlled <30%	51%
WLG Mt. Waliguan, China	36.28 N 100.90E 3.8	T	P	10	2005–2008	2005–2008	Sun	NC, GAW	controlled <40%	21%
LLN Mt Lulin, Taiwan	23.47 N 120.87E 2.9	T	P	10	2008–2009	2008–2009	Lin	NC, GAW	controlled <40%	25%

[a] More details in Table 2, T = TSI nephelometer, R = RR nephelometer, E = Ecotech nephelometer.
[b] More details in Table 2, A = Aethalometer, P = PSAP, M = MAAP.
[c] Contact listed is one (or more) of author list.
[d] Network ID: NB = NOAA baseline, NC = NOAA collaborative, EC = Environment Canada, EUSAAR = European Supersites for Atmospheric Aerosol Research, GAW = Global Atmosphere Watch, ABC = Atmospheric Brown Clouds project.
[e] Percent of data screened due to RH<95% criteria (at MBO used cloud flag).
[f] Multi-year aircraft profile measurements.

Author's personal copy

Author's personal copy

2.1.4. Southern Great Plains, USA (SGP)

The Southern Great Plains surface site in Oklahoma is operated by the US Department of Energy (DOE) and measurements of aerosol optical properties have been on-going since 1997 (Sheridan et al., 2001; Delene and Ogren, 2002). Between 2000 and 2007, a small, DOE-operated, instrumented light aircraft flew vertical profiles over the surface site 1–2 times per week, accumulating more than 750 profiles of aerosol scattering and absorption. A description of the first two years of measurements is presented in Andrews et al. (2004). The profiles were in the form of a descending stair step pattern with upper altitude level legs (1800–4600 m asl) approximately 10 min long and lower level legs (450–1500 m asl) approximately 5 min long. Here we assume the legs above 3000 m are in the FT, based on estimates of boundary layer height by Turner et al. (2001), and the FT statistics we present for SGP are from these higher altitude flight segments. The 'all data' statistics presented in Section 3 for SGP and BND include all level flight legs flown between 400 and 5000 m asl.

2.1.5. Bondville, USA (BND)

The Bondville surface site in Illinois is operated by the Illinois State Water Survey and aerosol optical property measurements have been made at the surface site by NOAA since 1996 (Delene and Ogren, 2002). Between 2006 and 2009 a small, instrumented airplane nearly identical to that at SGP flew regular profiles over or near the surface site accumulating 401 profiles. Many of the profiles were timed to match A-train overpasses with the intention of validating extinction measurements from CALIPSO. As with the SGP profiles, only legs above 3000 m asl were assumed to be in the FT. For both airplane data sets, the 10 minute level flight leg averaging time may result in noisier data than is found for the long-term hourly averaged data obtained at surface sites. The airplane data are also sparser than the continuous mountaintop measurements. There were typically 100–200 flights per year for each aircraft which generated a large number of vertical profiles, but the total sample time is still much shorter than that produced from continuous surface measurements.

2.1.6. Izaña, Spain (IZA)

The Izaña observatory is located in the Canary Islands on a volcanic mountain ridge spanning Tenerife. IZA is operated by the Meteorological State Agency of Spain. The observatory is well above (1–2 km, depending on the season) the top of the marine boundary layer. Local scale circulations induce strong diurnal cycles in water vapor, trace gasses and aerosol number concentrations (Rodríquez et al., 2009). The two most frequent synoptic patterns influencing the site are (a) northwesterly subsiding airflows from the North Atlantic which occur throughout the year and are associated with FT air and (b) east-southeasterly transport which occurs primarily in the summer (and sporadically in February and March) and is often laden with Saharan dust (Viana et al., 2002; Alastuey et al., 2005; Diaz et al., 2006). Maring et al. (2000) observed low scattering during NW air flows which they associated with pollutants, but found that up to 85% of the scattering was attributed to dust under Saharan-influenced flow regimes. Back trajectory analyses have also suggested that long range transport of pollution from North America and Europe may occasionally impact the site (Diaz et al., 2006; Maring et al., 2000). However, more recent work (Rodríguez et al., 2011) indicates that the climatology of anthropogenic aerosols at IZA is dominated by the arrival of North Africa air masses which bring a mixture of dust, including sulfate containing minerals (gypsum and anhydrite), and anthropogenic species (sulfate, ammonium and nitrate) linked to industrial emissions in North Africa and transported from the Mediterranean region.

2.1.7. Jungfraujoch, Switzerland (JFJ)

The Jungfraujoch high alpine research station is a Global Atmosphere Watch (GAW) global station; it is also part of the SwissMetNet network (MeteoSwiss) and of the Swiss National Monitoring Network for Air pollution (NABEL). Routine measurements of aerosol optical properties at JFJ began in 1995 by the Paul Scherrer Institute (PSI), although other aerosol properties were measured before that time (e.g., Baltensperger et al., 1991). Throughout the year the station is within clouds about 40% of the time. Therefore, ambient air is sampled from a total inlet, heated to 25 °C in order to evaporate cloud hydrometeors and to sample both their residual particles and the interstitial (or not activated) particles (Weingartner et al., 1999). Observations of the seasonal cycle of various aerosol parameters have found a minimum in winter and maximum in summer (Nyeki et al., 1998a,b; Baltensperger et al., 1997; Weingartner et al., 1999). JFJ can be considered as being in the FT during the entire day in winter; in spring during periods of synoptic subsidence it is influenced by planetary boundary layer air in the afternoon; and during summer boundary layer air systematically reaches the JFJ altitude during the afternoon, whereas the station stays in the FT during night (Lugauer et al., 1998; Baltensperger et al., 1997, Collaud Coen et al., 2011). Saharan dust events occur between 10 and 30 times per year generally in spring and autumn, leading to 250–650 h/year with mineral dust load (Collaud Coen et al., 2004). Because of the long time series of data available at JFJ, Collaud Coen et al. (2007) were able to examine long-term trends in aerosol optical properties.

2.1.8. Monte Cimone, Italy (CMN)

Atmospheric measurements at Monte Cimone in the northern Apennines have been made for more than a decade (Bonasoni et al., 2000). Measurements of light absorption began in 2005 (Marinoni et al., 2008) and routine light scattering measurements began in 2007. Here we use absorption data only from the start of the light scattering measurements to ensure data consistency (i.e., data corrections, see Section 2.3) with the rest of the sites in this study. Cristofanelli et al. (2009) describes the instrument installation at CMN. CMN is influenced by polluted air masses transported from both eastern and western Europe throughout the year and Saharan dust occasionally reaches the site in the spring and summer (Marinoni et al., 2008). CMN may also be impacted by biomass burning (forest fires) plumes from the Iberian Peninsula and northern Africa during the warmer months (Marinoni et al., 2008; Cristofanelli et al., 2009). The site experiences maxima in aerosol number and black carbon (BC) concentrations in the summer time likely due to enhanced vertical transport from lower elevations while in the winter negligible diurnal variations and low aerosol concentrations suggest CMN is in the FT (Marinoni et al., 2008). Except during periods of PBL influence, the CMN site is considered

Author's personal copy

representative of FT baseline conditions in the Mediterranean region (Bonasoni et al., 2000; Fischer et al., 2003).

2.1.9. Moussala Peak, Bulgaria (BEO)

The Basic Environment Observatory (BEO) is supported by the Institute for Nuclear Research and Nuclear Energy within the Bulgarian Academy of Sciences. Measurements of meteorological parameters began in 2003, measurements of greenhouse gasses (ozone, CO_2, NO_x), and trace gasses concentrations (CO, SO_2) began in 2006 (Angelov et al., 2011). Light scattering measurements began in 2007. Nojarov et al. (2009) studied ozone concentrations at BEO and saw differences in concentration depending on wind direction and time of day. They suggested the site had little boundary layer influence in the winter but transport from lower elevations was common in the summer.

2.1.10. Nepal Climate Observatory — Pyramid, Nepal (PYR)

Measurements at the Nepal Climate Observatory — Pyramid (NCO-P) began in 2006 in order to monitor the processes affecting global climate change and investigate how remote background sites are influenced by anthropogenic pollution. The site was established under the aegis of ABC-UNEP and SHARE-EV-K2-CNR. It is now a Global Atmosphere Watch (GAW) station. Bonasoni et al. (2008, 2010) present an overview of the measurements and the complex meteorological conditions at PYR. Marcq et al. (2010) describe the scattering and absorption measurements in more detail. The atmospheric measurements (e.g., aerosol optical properties) show a strong dependence on the meteorological conditions and diurnal cycles caused by upslope/downslope flow. The summertime monsoon results in clean conditions while the pre-monsoon period is the most polluted. Air masses sampled at the site come from the Indian subcontinent, the Arabian Peninsula and Persian Gulf and included dust, biomass burning and anthropogenic pollution as well as relatively clean air as source types. Marcq et al. (2010) identified 0500–0900 local time as representative of background (FT) conditions suggesting that earlier in the morning recirculation of previously lofted air could cause contamination and nucleation of new particles (Venzac et al., 2008).

2.1.11. Mount Waliguan, China (WLG)

Mount Waliguan is a GAW baseline observatory located on the north-eastern edge of the Qinghai-Xizang (Tibet) plateau in a dry arid region. More information about the station can be found in Zhou et al. (2003). Kivekas et al. (2009) investigated aerosol size distributions and number concentrations at WLG over a multi-year period. They observed higher concentrations in summer than other times of year, although there were extended periods of high concentrations in winter for one of the measurements. They explained the higher summer concentrations by noting that summer trajectories often passed over regional sources to the east (the cities of Xining and Lanzhou) while trajectories from the west passed over cleaner regions. Kivekas et al. (2009) did not observe a consistent diurnal pattern in wind direction, water vapor mixing ratio or accumulation mode aerosol for their period of study although diurnal wind direction changes have been observed for wind for other time periods (Wang et al., 2006). Kivekas et al. (2009) suggest it is difficult to identify times when WLG is in the FT.

2.1.12. Lulin Mountain, Taiwan (LLN)

The Lulin Atmospheric Background Station (LABS) was established to study the impact of air pollutants resulting from both regional sources and those arriving at the site via long range transport (http://lulin.tw/index_en.htm). Routine measurements of trace gasses, meteorological parameters, aerosol properties and solar radiation have been operational since 2006. In autumn of 2008 light scattering and absorption measurements were added to the suite of instruments at the site. LLN is subject to air masses influenced by southeast Asia biomass burning events (primarily in the spring), as well as air masses that have passed over China, India and cleaner maritime regions (particularly in the summer) (Chi et al., 2010; Lin et al., 2010). Summertime is also monsoon season. In 2009 the monsoon was extremely powerful, and a coupled typhoon Morakot struck Taiwan, resulting in huge landslides which caused tragic loss of life on the island and prevented access to LLN for much of the summer.

2.2. Measurements and instruments

The data used here consist of hourly-averaged, quality-checked light scattering and light absorption (where available) measurements from the ten mountaintop sites. For the two aircraft platforms light scattering and absorption values averaged over each level flight leg from every flight profile were used. Table 1 describes the relevant instruments operated at each site and further instrument details are listed in Table 2. In all

Table 2
Measurement description.

Scattering instrument	Total scattering wavelengths (nm)	Backscattering wavelengths (nm)	Corrections	Manufacturer info
TSI nephelometer, 3563	450, 550, 700	450, 550, 700	Anderson and Ogren (1998)	TSI, St. Paul, MN USA
RR nephelometer, M903	530	–	Anderson and Ogren (1998) (see Müller et al., 2009)	Radiance Research, Seattle, WA USA
EcoTech nephelometer, 9003	520	–	Müller et al. (2009)	EcoTech, Knoxville, Australia
Absorption instrument	**Absorption wavelengths (nm)**			
Aethalometer	370, 470, 520, 590, 660, 880, 950		Collaud Coen et al. (2010)	McGee Scientific, Berkeley, CA USA
PSAP	565 or 467, 530, 660		Bond et al. (1999) Virkkula et al. (2005)[a]	Radiance Research, Seattle, WA USA
MAAP	670 (635 meas)		Müller et al. (2011)	Thermo, Fischer-Scientific Franklin, MA USA

[a] At MBO the scattering response function from Virkkula et al. (2005) was used.

Author's personal copy

cases light scattering was measured by integrating nephelometers, and at least one channel measured at a green wavelength (in the range 520–550 nm). Light absorption was measured by various filter-based measurements (i.e., particle soot absorption photometer (PSAP), aethalometer, multi-angle absorption photometer (MAAP)). Most but not all absorption measurements also included a green wavelength channel.

From the measurements of light scattering (σ_{sp}) and light absorption (σ_{ap}) the following parameters can be calculated (Delene and Ogren, 2002; Andrews et al., 2006):

$$\text{Light extinction } \left(\sigma_{ep}\right),\ \sigma_{ep} = \sigma_{sp} + \sigma_{ap} \quad (1)$$

$$\text{Single scattering albedo } (\omega_o),\ \omega_o = \sigma_{sp}/\sigma_{ep} \quad (2)$$

$$\text{Ångström exponent } (\text{å}),\ \text{å} = -\ln\left(\sigma_{sp,1}/\sigma_{sp,2}\right)/\ln(\lambda_1/\lambda_2) \quad (3)$$

$$\text{Backscatter fraction } (b),\ b = \sigma_{bsp}/\sigma_{sp} \quad (4)$$

$$\text{Asymmetry parameter } (g),\ g = -7.14^{*}b^3 + 7.46^{*}b^2 - 3.96^{*}b + 0.9893 \quad (5)$$

where $\sigma_{sp,i}$ is the scattering coefficient at wavelength i, λ_i is the wavelength i and σ_{bsp} is the backscattering coefficient (σ_{bsp} is measured by all of the TSI nephelometers included in this study). Unless otherwise noted aerosol optical properties are reported at 550 nm and the Ångström exponent values are calculated using the 550 nm and 700 nm wavelength pair. The measured parameters (σ_{sp} and σ_{ap}) and σ_{ep} are extensive aerosol properties; they depend on the amount of aerosol present. Single scattering albedo, the scattering Ångström exponent, the backscatter fraction, and the asymmetry parameter are independent of the amount of aerosol present—they are termed aerosol intensive properties.

Both backscatter fraction and Ångström exponent provide information about the size distribution of the aerosol particles in an air mass. Backscatter fraction provides information about the small end of the size distribution while Ångström exponents are used to identify the presence or absence of large aerosol particles such as dust or sea-salt. Collaud Coen et al. (2007) present a detailed discussion about the size distribution dependence of both of these parameters. They show (their Fig. 7), for submicron aerosol particles, that the backscatter fraction is most sensitive to the smallest accumulation mode particles, i.e., diameter<0.4 μm, while the wavelength dependence of scattering efficiency (i.e., Ångström exponent) is most sensitive to particles in the 0.5–0.8 μm diameter range. Delene and Ogren (2002) show the importance of coarse (diameter>1 μm) mode aerosol in controlling the Ångström exponent by presenting the relationship (their Fig. 9) between fine mode scattering fraction (ratio of scattering for diameter<1 μm/scattering for diameter<10 μm) and Ångström exponent. Thus changes in back-scatter fraction and Ångström exponent reflect changes in different parts of the size distribution and, depending on the shape of the aerosol size distribution, backscatter fraction might increase, decrease or not change when the Ångström exponent changes and vice versa.

2.3. Data consistency

A main goal of this paper is to compare and contrast the FT aerosol optical property observed at various sites, thus measurement consistency is critical. All measurements presented here are adjusted to standard temperature and pressure (STP, $T_{standard} = 273.15$ K and $P_{standard} = 1013.25$). The instruments are typically operated at low relative humidity (<40%). Many sites use humidity control techniques (e.g., heaters) to ensure that the sample air is at low RH; however, at sites where the humidity is not controlled the difference between ambient (outside) temperature and lab temperature usually ensures low RH conditions within the instruments. Table 1 specifies whether the site utilizes RH control and provides the typical RH values of the sample air. The scattering coefficient at low RH can differ substantially from scattering at ambient conditions, which in turn can influence the derived aerosol optical properties (e.g., single scattering albedo).

Almost all instruments had a measurement at or near 550 nm so comparisons were done at this wavelength. The single wavelength MAAP absorption measurements were adjusted to 550 nm from their original measurement wavelength utilizing a $1/\lambda$ dependence, e.g., $\sigma_{ap,550} = \sigma_{ap,\lambda}{}^{*}(550/\lambda)$. The assumption of absorption having a $1/\lambda$ dependence is based on the 'small particle limit' theory (van der Hulst, 1957) and assumes small (d ~ 0.02 μm) spherical particles with constant index of refraction. It has been found to be fairly representative of atmospheric aerosol (e.g., Bergstrom et al. (2002)). The spectral PSAP and aethalometer measurements were adjusted from 567 to 550 nm using the absorption Ångström exponent which is calculated similar to the scattering Ångström exponent (Eq. (3)) but uses absorption values in place of scattering.

The single wavelength nephelometer measurements at 520 nm (Ecotech nephelometer at CMN) and 530 nm (Radiance Research nephelometer at MBO) were not adjusted to 550 nm as the simple $1/\lambda$ dependence does not apply to scattering aerosol. The magnitude of the scattering wavelength adjustment can be estimated based on an assumed Ångström exponent (å). If one assumes that $\text{å} = 2$, the 520 nm scattering would decrease by ~11% when shifted to 550 nm as calculated using the following equation:

$$\sigma_{sp,550} = \sigma_{sp,520}{}^{*}(520/550)^{\text{å}}. \quad (6)$$

A smaller Ångström exponent would result in a smaller wavelength adjustment and vice versa. As shown later, the value of the median Ångström exponent at most sites is between 1 and 2.

Another issue affecting data consistency is the instrument specific corrections applied to the data. All TSI nephelometer data were corrected for light source and angular non-idealities utilizing the method described in Anderson and Ogren (1998) which incorporates an Ångström exponent adjustment to account for particle size. In a nephelometer inter-comparison paper Müller et al. (2009) suggested that the single wavelength Radiance Research nephelometer had correction parameters quite similar to the TSI nephelometer, thus we applied the Anderson and Ogren corrections to the Radiance Research nephelometer at MBO. The Anderson and Ogren corrections were also applied to the single wavelength Ecotech nephelometer at CMN — we utilized the sub-micron correction factors for

Author's personal copy

550 nm based on the assumption that there would be few super-micron particles in the FT except during dust events. Müller et al. (2009) suggest Ecotech nephelometer-specific adjustments, however without information about the specific size distribution the appropriate correction factor was unclear.

The PSAP measurements were corrected using the Bond et al. (1999) method which takes into account differences in manufacturer default values and the influence of scattering on absorption. The Bond et al. (1999) correction was developed specifically for the 1-wavelength version of the PSAP; Ogren (2010) suggests how these corrections may be applied to the 3-wavelength version of the instrument and that procedure was followed here. The MBO PSAP was an exception — the Bond et al. (1999) corrections for spot size, and flow were applied, but the Virkkula et al. (2005) scattering response function was utilized to correct for scattering. For the JFJ aethalometer data, the Weingartner et al. (2003) correction was applied ($R=1$), however a multiple scattering correction factor of $C=2.81$ was used as suggested by Collaud Coen et al. (2010). The MAAP has a built-in adjustment for the light scattering artifact (Petzold et al., 2005) so aside from STP adjustment the only 'correction' applied to the MAAP data was the assumption that the instrument wavelength was 637 nm rather than the manufacturer's stated measurement wavelength of 670 nm based on Müller et al. (2011). This wavelength change affected the magnitude of the absorption adjustment to 550 nm.

2.4. FT identification

As described in the introduction, a major advantage of mountaintop observatories is the opportunity they provide to conduct long-term measurements in the FT. However, depending on observatory location, topography and meteorology, several mechanisms can cause the upward movement of lower elevation air resulting in boundary layer (BL) influenced sampling conditions described in more detail below. Additionally, once BL air has reached the FT (by whatever process), it may remain in the region for extended periods of time (hours to days) depending on the meteorological conditions (e.g., Gallagher et al., 2011; Collaud Coen et al., 2011; Marcq et al., 2010; Lugauer et al., 1998). The presence of such residual layers makes it difficult to rigorously define FT air. Because these residual BL influenced layers are the result of local conditions the FT aerosol should be considered regional rather than global in nature.

The location, height and steepness (topography) of the mountain all play a role in determining the strength and frequency of the diurnal wind patterns (Kleissl et al., 2007). Local thermally-driven flow is a particularly important method for BL air masses to be transported to sites that would otherwise be located in the FT (Mendonca, 1969). During the day insolation heats the air at lower elevations resulting in flow up the side of the mountain, and at night the flow reverses as temperatures decrease. Thermally-driven flow has been shown to cause strong diurnal cycles in aerosol loading (e.g., Bodhaine, 1983), gas concentrations (e.g., Sheu et al., 2010) and water vapor mixing ratio (e.g., Weiss-Penzias et al., 2006). The typical diurnal pattern has concentrations (of aerosol, trace gas or water vapor) at their peak in the afternoon while lower values are observed in the early morning hours during downslope flow of FT air. (Ozone and some other gaseous species may depart from the typical diurnal pattern due to chemical production and, in the case of ozone, subsidence from upper troposphere and/or lower stratosphere (e.g., Cristofanelli et al., 2010).) Because of the consistency of the diurnal cycles at many mountain locations, time of day has been used as an indicator of when the site is in the FT (Bodhaine, 1983; Nyeki et al., 1998a; Marcq et al., 2010; Sheu et al., 2010; Shaw, 2007; Marinoni et al., 2008).

Unfortunately (for simplicity of analysis), disruptions to thermally-driven, upslope/downslope flow are quite common due to transport mechanisms occurring on larger (e.g., synoptic) spatial scales. Convective conditions and seasonal variability can compromise the ability of a time window to represent FT air (Lugauer et al., 1998; Gallagher et al., 2011; Collaud Coen et al., 2011). Fig. 2 shows the diurnal pattern of normalized light scattering as a function of season for the ten mountaintop sites. Three sites in this study (MLO, IZA and LLN) have strong (large amplitude) diurnal cycles indicative of thermally-driven flow throughout the year. Another site (PYR) has strong diurnal cycles for all seasons except summer when monsoon circulation sets in (Bonasoni et al., 2010; Marcq et al., 2010; Marinoni et al., 2010). These four sites are the lowest latitude sites (<30°N) in this study and their diurnal patterns are consistent with the suggestion by Kleissl et al. (2007) that mountains at lower latitude would have stronger thermal patterns due to stronger insolation. The diurnal cycles at the other sites in Fig. 2 are less regular. In winter, most of the higher latitude sites (JFJ, CMN, BEO, WLG) show minimal variability over the day with only a hint of a thermally-driven diurnal pattern while WHI and MBO appear to have no well-defined pattern in winter. Baltensperger et al. (1997) suggested that the lack of a diurnal pattern in the wintertime aerosol signal can likely be attributed to the air masses measured at the site being decoupled from the polluted boundary layer. Similar seasonal changes in diurnal cycles of condensation nuclei (CN) concentrations at some mountain sites have been observed (Gallagher et al., 2011; Venzac et al., 2009; Nyeki et al., 1998b, Marinoni et al., 2008), although wintertime boundary layer intrusions are possible under certain conditions (e.g., Gallagher et al., 2011; Collaud Coen et al., 2011). The seasonality of the diurnal cycle at WLG is different than the other sites — in the winter it is similar to other high latitude sites (JFJ, CMN, BEO) as mentioned above, but summertime suggests no diurnal pattern in light scattering while in spring and fall the scattering peaks several hours earlier than the other sites. This lack of a strong diurnal cycle at WLG is consistent with the observation by Kivekas et al. (2009) that it is difficult to identify periods of FT air at the WLG observatory.

The annual monsoon observed at PYR is an example of seasonal large scale circulation changes that can affect local, insolation-induced diurnal cycles. Shorter term disruptions can also occur. For example, dynamical lifting related to synoptic scale weather patterns (fronts, cyclonic motion, etc.) (Lugauer et al., 1998) can also cause vertical transport of boundary layer air masses, as can mechanically-forced lifting which occurs when lower altitude winds are fast enough to push the air up the side of the mountain (Kleissl et al., 2007; Venzac et al., 2009). While "tracer" alternatives to time of day and in-depth meteorological analysis for FT identification have been suggested (e.g., RH/water vapor mixing ratio (e.g., Weiss-Penzias et al., 2006)) Lugauer et al. (1998) suggest these alternatives

Author's personal copy

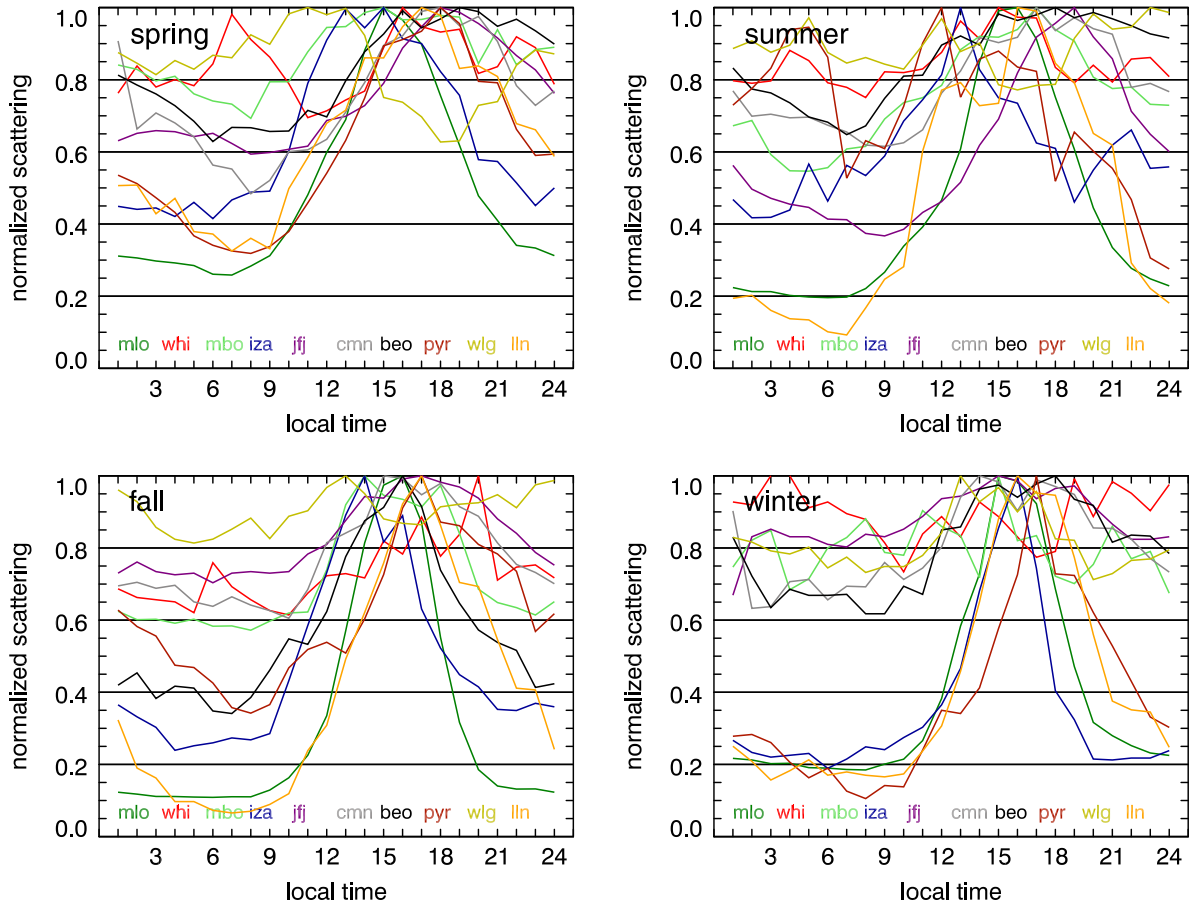

Fig. 2. Diurnal cycles of normalized scattering at each mountain site as a function of season; spring = MAM, summer = JJA, fall = SON, winter = DFJ. MBO scattering from Radiance Research nephelometer which operated year-round.

are often not robust at sites like JFJ because the topography (i.e., whether the mountain stands alone (e.g., MLO) or is situated within a range (e.g., WHI)) and the "advection direction of the synoptic scale horizontal wind" will control whether a mountain site is measuring BL or FT air. The type of local meteorological analysis required to determine the degree to which a site is in the FT requires information beyond what is typically measured at the individual mountain sites and is thus outside the scope of this paper.

Recognizing the limitations of broadly applying a simple time of day approach, there are two other related approaches which could also be used to identify FT air: (a) time of day for winter data only and (b) time of day for all days with strong diurnal cycles. The first takes advantage of the wintertime decoupling from the boundary layer observed at several sites and assumes all wintertime air is representative of the FT. Because the lower latitude sites (MLO, IZA, PYR, LLN) still have thermally-driven flow in the winter, a further time constraint limiting data to early morning hours is required so that this method is applicable to all sites in this study. A major limitation of this approach is that using only wintertime data results in missing any seasonal changes in FT aerosol loading due to changes in sources and source regions (for example, springtime dust transport or summertime biomass burning) and/or caused by enhanced boundary layer exchange (i.e., during the summer) (Venzac et al., 2009; Liu et al., 2008b). The second approach, suggested by Baltensperger et al. (1997), was most recently used by Gallagher et al. (2011) to identify the frequency of boundary layer influence at WHI. Gallagher et al. (2011) fit a sinusoidal function to 1 year of WHI particle number concentration measurements in order to identify days with strong diurnal cycles and, hence, BL influence. Using this method, boundary layer intrusions at WHI occurred 10–50% of the time depending on the month, but they note that this is a conservative approach as there are other ways for BL air to be transported vertically. This sinusoidal fit method could also be used as a conservative means of identifying FT air, i.e., by limiting the FT analysis to days with strong diurnal cycles in aerosol scattering and selecting a narrow early morning time window when downslope flow would likely be representative of FT air. Limitations of this approach include (a) wintertime air masses are often decoupled from the BL and thus may not show a diurnal cycle and, hence, would not be identified as FT air and (b) long range transport in the FT (e.g., dust) may also affect the shape of the diurnal cycle, resulting in the exclusion of those days from the analysis and thus potential exclusion of significant FT events. Without doing the detailed meteorological analysis it is impossible to determine which of these three approaches (time of day, winter + time of day, sinusoid fit + time of day) results in the best representation of FT air at each site and each has advantages and disadvantages. Thus, aware of its limitations, the simplest method — using only the time of day approach — is used here. Data collected between 3 am and 9 am local time was classified as FT air; this criterion appears to be reasonable for most sites and seasons based on the diurnal patterns of light scattering presented in

Author's personal copy

Fig. 2; WLG is the exception as the timing of the diurnal cycle there changes from season to season — at WLG the time of day based approach may only be appropriate in the winter.

2.5. Screening for local cloud influence

The final step taken for data consistency is an attempt to remove local cloud effects from the data sets. Clouds are a source of inconsistency because they have the ability to scavenge aerosol particles (e.g., Hampl et al., 1971; Hegg and Hobbs, 1983), resulting in lower aerosol loading. Cloud scavenging effects have been described at some of the sites in this study: Marinoni et al. (2008), Nyeki et al. (1998b), and Weingartner et al. (1999). In addition, cloud scavenging may preferentially remove larger hygroscopic particles while leaving smaller particles in the interstitial air. As soot tends to exist in the smaller particles (at least for recently emitted aerosol) (Putaud et al., 2004; Hitzenberger et al., 2006), cloud scavenging may result in the non-scavenged aerosol having a lower single scattering albedo (e.g., Berkowitz et al., 2011; Marcq et al., 2010; Sellegri et al., 2003). A thorough discussion of changes in optical properties due to cloud scavenging is beyond the scope of this paper. Some sites are equipped with so-called "whole air inlets" but very few can provide a satisfactory sampling efficiency curve in particular for large cloud droplets. We therefore decided to apply a more conservative criteria based on relative humidity. To eliminate data during local cloud presence, data were included in this analysis when the local ambient relative humidity was less than 95%; Marinoni et al. (2008) used a similar criterion at CMN. Note: this RH restriction may not exclude data when ice clouds are present at the site. RH data were unavailable for BEO so the BEO data are not cloud screened. BEO is, however, one of the sites equipped with a whole air inlet and therefore the cloud artifact is minimized. For MBO the 'no-cloud' data flag provided was used — this flag is based on both a sheltered and non-sheltered relative humidity measurement at the site, and it accounts for riming conditions. The effect of this cloud screening process was small increases in median aerosol absorption and scattering for most sites in both the 'all data' and 'FT data' categories compared to data without a cloud screening constraint. The single scattering albedo was also slightly higher in the cloud-screened data for most sites. The largest changes in scattering and absorption due to removal of data when RH>95% occur at WHI, MBO, JFJ, CMN and PYR. These are also the sites most frequently in-cloud, i.e., with the largest fraction of data having RH>95%. Table 1 lists the percentage of data removed by cloud screening.

3. Results/discussion

3.1. Annual climatologies

Fig. 3 shows annual climatological values for six aerosol optical properties at each site both for 'all data' and data that has been identified as being FT aerosol using the 3 am≤FT≤9 am local time criterion (for the airplane data from SGP and BND the flight altitude was used to identify FT air — there was no time constraint). For both 'all data' and 'FT data' we have screened out the cloud influence from the data as discussed above. The 5th percentiles for some of the extensive properties at some of the sites were not plotted. This reflects reported measurements below zero, which occurred during very clean conditions where the aerosol property being measured was below the detection limit of the instrument. The data in Fig. 3 are plotted from west to east so that the six western hemisphere sites are on the left side of the plot and the eastern hemisphere sites are on the right side of the plot. We maintain this convention throughout the paper. There are several notable features in Fig. 3.

First, there are 2 orders of magnitude difference in the median values of light absorption and 1 order of magnitude difference in light scattering and light extinction from the cleanest FT air (MLO) to the FT air with the highest aerosol loading (WLG). In other words there is significant variability in FT aerosol loading among the locations.

Second, the extensive aerosol properties shown in Fig. 3abc tend to increase from west to east (taking MLO as the western most point). This is true for both 'all data' and 'FT data' and suggests that the BL and FT are coupled and/or that the time of day screening for FT air may not be ideal. This west to east increase in extensive properties roughly corresponds with increases in population density and estimates of global surface PM2.5 (van Donkelaar et al., 2010); it may also be related to proximity to aerosol sources such as desert dust or biomass burning.

Third, the extensive property values almost separate by eastern and western hemisphere in both the full dataset and the FT subset: MLO through BND plus JFJ tend to have lower values — less aerosol, while IZA plus CMN through LLN tend to have higher values. IZA likely falls out of order in the west to east gradient because its proximity to Africa means it is often strongly influenced by dust emissions from the Sahara desert (Maring et al., 2000; Alastuey et al., 2005; Diaz et al., 2006). Liu et al. (2008b) present maps showing the frequency of dust influence as a function of season and altitude for different regions of the globe. IZA is clearly more impacted by African outflow than the European sites nearest to it (JFJ, CMN, BEO) (see Liu et al. (2008b), Figs. 2 and 5). The north to south European gradient (IZA, JFJ, CMN, BEO) in in-situ extinction is consistent with results from lidar measurements for ten sites in the European Aerosol Research Lidar Network (EARLINET). Matthias et al. (2004) observed a north/south increase in lidar-derived extinction in the 2–5 km altitude range that they suggested was caused by more exposure to African dust for the southern sites (see Matthias et al. (2004), their Fig. 6). There was no north to south gradient in aerosol amount if all 12 sites were considered, nor was there a consistent pattern in aerosol amount based on observatory altitude.

Finally, at most sites, there is a decrease in the 'FT data' aerosol absorption, extinction and scattering compared to 'all data' (Fig. 3). Sites with stronger diurnal cycles (MLO, IZA, PYR, LLN; Fig. 2) tend to have larger decreases in FT aerosol loading compared to their 'all data' aerosol loading, reflecting the time of day FT segregation used here. The extensive properties for the two airplane platforms (BND, SGP) also show a large difference between 'all data' and 'FT data'. As mentioned in the site descriptions, at BND and SGP the 'all data' values are determined using measurements over the entire flight profile (between 400 and 5000 m asl), thus the 'all data' measurements are always strongly influenced by boundary layer air. For the sites with little indication of diurnal cycle in scattering (WHI, WLG), there is very little difference between FT air and the entire data set.

Author's personal copy

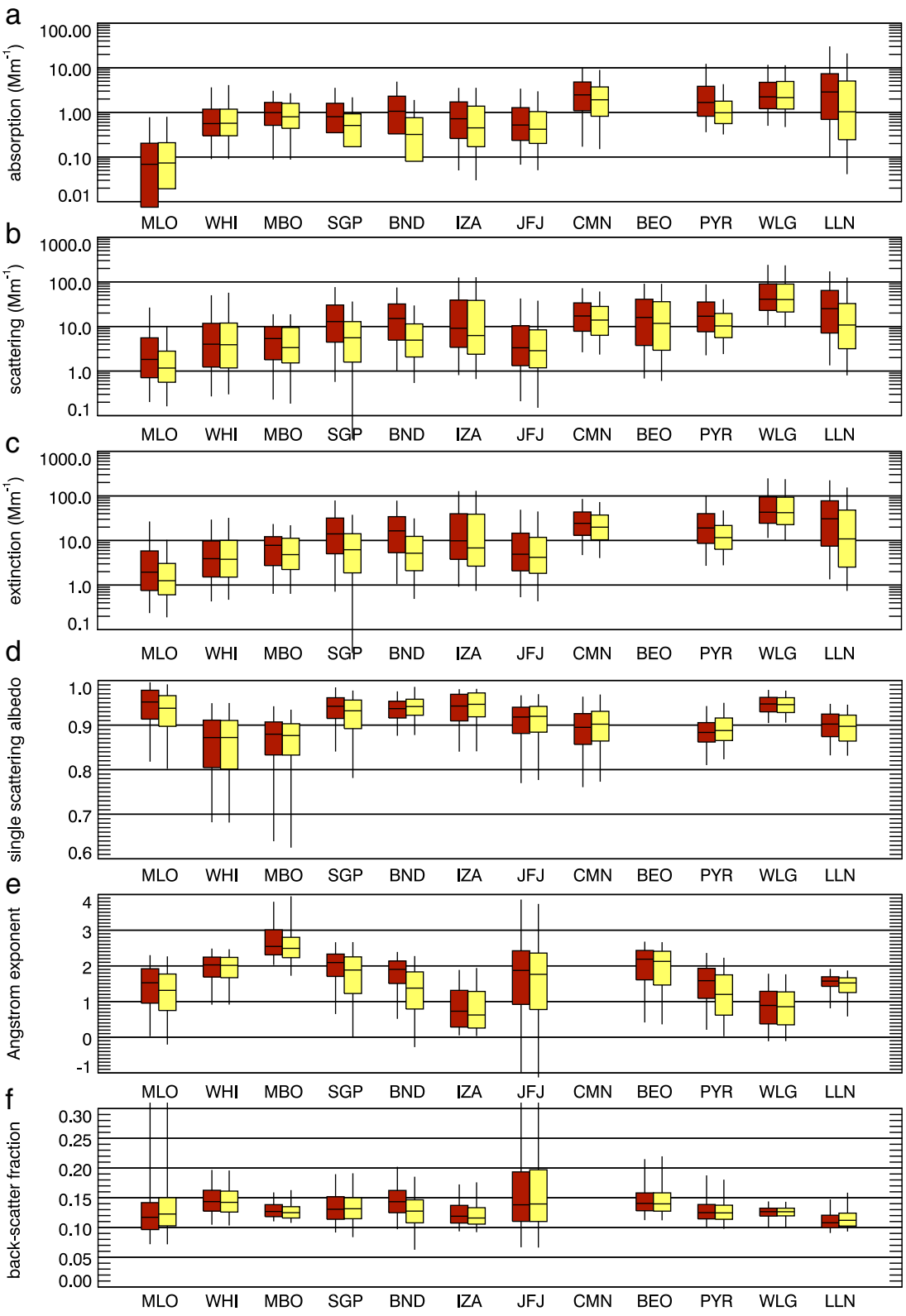

Fig. 3. Aerosol optical properties for 'all data' and FT-only data. Data are reported at 550 nm, except at CMN where light scattering is at 520 nm. Red = all data, Yellow = FT data (based on time of day). Horizontal line is the median (50th percentile), edges of box are 25th and 75th percentiles, whiskers are 5th and 95th percentiles. Single scattering albedo, Ångström exponent and backscatter fraction are calculated with the constraint light scattering >1 Mm^{-1} to minimize noise caused by taking ratio of two small numbers. Ångström exponent is calculated for 550/700 nm pair.

Lidar extinction values based on long-term measurements can be compared with the in-situ extinction values reported here for 'FT data' periods if the lidar observations are segregated by altitude. In Matthias et al. (2004) the 2–5 km altitude subset of data is the most analogous to the 'FT data' in this study. Using 10 lidar sites across Europe they found mean values of aerosol extinction at ~351 nm to range between 20 and 70 Mm^{-1}. This is equivalent to ~8–30 Mm^{-1}

Author's personal copy

at 550 nm if an Ångström exponent of 2 is assumed, and equivalent to ~10–35 Mm^{-1} at 550 if an Ångström exponent of 1.5 is assumed. Mattis et al. (2004) found a mean FT (below 5 km) extinction value at 532 nm of 7.4 ± 8.4 Mm^{-1} for measurements made over Leipzig. Median values of FT in-situ extinction are ~3 Mm^{-1} at JFJ and ~20 Mm^{-1} at CMN. The median value of FT in-situ scattering (which is a reasonable surrogate for FT extinction) at BEO is ~10 Mm^{-1}. Thus, the lidar observations and the in-situ aerosol observations show a similar magnitude of aerosol light extinction over Europe. On a housekeeping note relevant to these comparisons, recall that the in-situ data presented in this paper are reported at STP and low RH rather than ambient conditions. For the purposes of comparing with lidar (and satellite) measurements the assumption can be made that the STP and RH adjustments counteract each other, to some extent. A measurement at STP conditions will decrease by approximately 1.4 when adjusted to the pressure representative of 2.5 km altitude. Typical hygroscopic growth factors will increase the dry scattering by a factor of 1–3 at 80% humidity (e.g., Fierz-Schmidhauser et al., 2010; Carrico et al., 2003). The extent to which STP and aerosol hygroscopicity counteract each other at any specific site will, of course, depend on the site location and aerosol composition. In Section 3.1 further lidar/in-situ extinctions comparisons are performed and in Section 3.2 the high altitude in-situ FT extinction values are compared with satellite observations.

Fig. 3def show differences in intensive aerosol properties among mountaintop sites. Only data where scattering at 550 nm was greater than 1 Mm^{-1} was used in the calculation of the intensive properties. While this biases the data towards less clean conditions at some of the more pristine sites, it also eliminates some of the noise produced by taking the ratio of two small numbers. The three sites with the most absorbing aerosol (lowest single scattering albedo) are WHI, MBO and PYR (Fig. 3d). Transport of Asian aerosol (dust and pollution) has been observed at WHI in the spring (Leaitch et al., 2009; McKendry et al., 2007) and the site is frequently impacted by regional forest fire smoke primarily during the summer (Gallagher et al., 2011; McKendry et al., 2011). PYR receives significant anthropogenic pollution and biomass burning (Marcq et al., 2010). The MBO measurements are for the springtime dust season, so it is unlikely that the low single scattering albedo is due to regional forest fire smoke, however both biomass burning and pollutant aerosol transported from Asia have been observed at the site during the springtime (Weiss-Penzias et al., 2007; Fischer et al., 2010). The indication of darker aerosol at MBO could also be biased by the 1 μm size cut (absorbing aerosol tends to be predominately in the sub-micron fraction (e.g., Delene and Ogren, 2002; Hitzenberger et al., 2006; Putaud et al., 2004)).

Comparing the shift in single scattering albedo between 'all data' and 'FT data' for each location suggests the sites can be grouped into three categories. In the first group (MLO, MBO, SGP and LLN), the 'FT data' single scattering albedo is lower than for 'all data'. Of the mountain sites, the MLO data exhibits the largest change in median single scattering albedo between 'all data' and 'FT data' single scattering albedo. This likely reflects the difference between the higher single scattering albedo, marine-influenced aerosol sampled during upslope conditions and aged pollution aerosol that has been transported through the FT to MLO. A similar explanation is likely the case for MBO and LLN, although the upslope aerosol at these two sites is unlikely to have a marine influence. The lower FT single scattering albedo of the SGP aerosol has been suggested to be due to cloud processing (Andrews et al., 2004). In the second category, the median single scattering albedo is higher for 'FT data' than 'all data'. The data from IZA, JFJ, CMN and PYR and BND fall into this group. The likely explanation for the lower single scattering albedo in 'all data' is that the boundary layer air which reaches the sites in the afternoon is more polluted and includes relatively more absorbing aerosol (e.g. particles produced by combustion such as diesel soot or biomass smoke) than the FT air. In addition, these four sites are influenced, (to varying extent) by the long range, free tropospheric transport of dust from the Sahara (IZA, JFJ, CMN) and Indian subcontinent/Arabian peninsula (PYR) as described in the individual station sections. Dust tends to be associated with higher single scattering albedo values than pollution/biomass aerosol, as will be discussed in Section 3.3. A similar explanation (more polluted BL air) may cause the observed increase for FT single scattering albedo at BND, although it may also be due to dust — the decrease in median Ångström exponent at BND between 'all data' and 'FT data' is the largest observed at any of the sites (Fig. 3e). Finally, the single scattering albedo statistics at some sites (WHI and WLG) are quite similar for both 'FT' and 'all data'.

Fig. 3e shows changes in the scattering Ångström exponent for 'all data' versus 'FT data'. The Ångström exponent is inversely related to particle size and the Ångström exponent at MBO is significantly higher than at the other sites due to a 1 μm diameter size cut upstream of the nephelometer. Excluding MBO, the aerosol particles at BEO have the highest Ångström exponent (median å>2) suggesting a significant influence of anthropogenic fine-particle pollution. The aerosol particles at WLG and IZA have the lowest Ångström exponent values (median å<1) suggesting that of all the sites they may be the two most strongly influenced by dust. Most sites show a decrease in Ångström exponent for the FT air, indicative of the presence of larger particles in the FT. This decrease in Ångström exponent may suggest the presence of a free troposphere background dust aerosol and is consistent with GOCART results that show a large contribution from dust at 3 km for most regions in most seasons (Yu et al., 2010). Other explanations include: (a) the boundary layer may have a higher contribution from sub-micron aerosol particles (i.e., lower Ångström exponent) as a result of the many sub-micron aerosol sources at the surface and (b) aging of the FT aerosol during transport may result in an increase in particle size due to coagulation and/or gas to particle conversion on existing particles.

Fig. 3f compares backscatter fraction for 'all data' and for 'FT data'. For all locations the median backscatter fraction value falls in a narrow range between 0.1 and 0.15. The highest median values of backscatter fraction are observed at WHI, JFJ and BEO, while the lowest are found at MLO, IZA and LLN. This hints at a north/south gradient in backscatter fraction with the higher latitude sites having more of a contribution from accumulation mode particles. The backscatter fraction data at JFJ are twice as variable as those measured at any of the other stations, based on the values of the 25th and 75th percentiles, although the median values are

Author's personal copy

consistent with the other sites. Most sites (WHI, SGP, JFJ, BEO, PYR and WLG) see little or no change between backscatter fraction in 'FT data' versus backscatter fraction for 'all data'. At two sites (MBO, IZA) there is a slight decrease in backscatter fraction for the FT aerosol compared to the entire data set, suggesting a size distribution shift away from smaller accumulation mode particles in the FT, while at BND the decrease in backscatter fraction is quite large. In contrast, at MLO and LLN there is a noticeable increase in backscatter fraction in the 'FT data' implying an increase in smaller particles relative to 'all data'. Mie theory predicts that backscatter fraction should be higher for fine mode spherical aerosol particles; however, several studies have found backscatter fraction values to be higher for dust than other types of aerosol particles (Carrico et al., 2003; Doherty et al., 2005). Doherty et al. (2005) suggested that changes in backscatter fraction can also be driven by particle shape and that we may not fully understand the uncertainty associated with corrections applied to the nephelometer data. This suggests that backscattering fraction may not be a robust indicator of particle size, particularly for data at low RH conditions where particle sphericity is not assured.

3.2. Monthly climatologies

Fig. 4 presents monthly climatologies of various FT aerosol properties at each site. There are also horizontal lines on each plot indicating site median seasonal values. Most parameters show seasonal variability; however, that is not the case for all sites and all aerosol optical properties. Below we discuss each optical property in more detail. As with Fig. 3, only data where scattering at 550 nm was greater than 1 Mm^{-1} were used in the calculation of the intensive properties.

3.2.1. Extensive properties — light absorption, light scattering and light extinction

Light scattering and absorption tend to track each other at most sites suggesting common sources for scattering and absorbing aerosol (Fig. 4ab). Aerosol loading tends to be highest in the spring and/or the summer (Fig. 4abc) at all sites. MLO and LLN have distinct springtime peaks due to transport from Asia at MLO (Perry et al., 1999) and biomass burning influence at LLN (Chi et al., 2010; Lin et al., 2010). Extensive properties at JFJ, CMN and BEO peak in the summer, while many of the other sites have broad or even bi-modal peaks encompassing spring and summer (WHI, SGP, BND, IZA and WLG). The spring/summer increases in extensive properties are likely related to enhanced boundary layer influence on the FT caused by increases in boundary layer height and stronger upslope transport due to increased insolation. At PYR the June increase in intensive properties is due to an intense transport of dust mixed with pollution during a break in the monsoon. The monsoon at PYR brings high humidity and precipitation during July and August, and the cloud free constraint (RH<95%) screened all but two data points from inclusion in Fig. 4. Therefore, at PYR, there is only a line rather than a box-whisker drawn for these months. The bimodal patterns observed at some sites are representative of changing sources and/or circulation. For example, IZA has peaks in dust aerosol in spring and summer (Diaz et al., 2006).

There are a few anomalous months at some stations. The high extensive property spike in March at IZA is likely due to strong outflow from northern Africa (Liu et al., 2008b; Diaz et al., 2006). The high scattering and absorption observed in January at WLG is difficult to explain. This increase in scattering aerosol corresponds to a decrease in backscatter fraction (Fig. 4f) suggesting the aerosol being sampled is in the middle to upper part of the 0.1–1 μm size range, but there is no corresponding decrease in Ångström exponent that would suggest an incursion of coarse mode dust aerosol particles. Kivekas et al. (2009) measured condensation nuclei (CN) concentrations at WLG over a 2.5 year period between 2005 and 2007. They noted higher concentrations of CN in December 2005–January 2006, but did not observe the same phenomenon the following year and were unable to explain it.

Fig. 4c is similar to Fig. 4a because extinction is dominated by light scattering at all locations. We include extinction here for comparisons with remote sensing measurements of extinction. EARLINET lidar climatologies of FT extinction have been described for various locations in Europe (de Tomasi et al., 2006). They report spring/summer extinction (532 nm) at 3 km over SE Italy to be approximately 30 Mm^{-1} in the spring/summer and 10 Mm^{-1} in the fall/winter. These values are remarkably similar to the FT seasonal extinction values seen here for CMN. Barnaba et al. (2010) present monthly lidar extinction profiles for the Po Valley in northern Italy showing the broad spring/summer time increase in extinction that is seen at CMN. Again the lidar extinction values at the altitude of CMN are quite similar to the extinction measurements.

3.2.2. Single scattering albedo

Although light scattering and absorption generally track each other, there are differences in the relative proportions of scattering and absorbing aerosol over the course of the year resulting in variations in single scattering albedo over the annual cycle. At many sites the single scattering albedo tends to be lower and noisier in the winter (Fig. 4d) when the air is the cleanest. These lower values of single scattering albedo suggest the aerosol is relatively more absorbing. These lower values may be due to bias in the measurements at low aerosol loadings, an increase in sources of absorbing aerosol (e.g., wood smoke from heating or fuel combustion), and/or preferential cloud scavenging of scattering aerosol (e.g., Marcq et al., 2010) and/or slower secondary aerosol formation due to lower light intensity. WLG is an exception — there the lowest

Fig. 4. Monthly climatologies of FT aerosol optical properties at each site: (a) absorption, (b) scattering, (c) extinction, (d) single scattering albedo, (e) Ångström exponent, (f) backscatter fraction. Box-whiskers show percentiles as described in Fig. 3. Data are reported at 550 nm, except at CMN where light scattering is at 520 nm and MBO where light scattering is at 530 nm (all other MBO plots are at 550 nm). Single scattering albedo, Ångström exponent and backscatter fraction are calculated with the constraint light scattering >1 Mm^{-1} to minimize noise caused by taking ratio of two small numbers. The horizontal red bars behind the box-whiskers are the seasonal median values where the four seasons are defined as spring (MAM), summer (JJA), fall (SON) and winter (DJF). For ease of comparing the intensive parameters among stations despite the different y-axis ranges, an orange line has been drawn at a constant value on each plot (0.90 for single scattering albedo, 1.5 for Ångström exponent and 0.12 for backscatter fraction). Note: the MBO scattering plot uses RR nephelometer data (530 nm) which operated year round, all other MBO plots utilize the TSI nephelometer data (550 nm) which was only operated in the springtime.

Author's personal copy

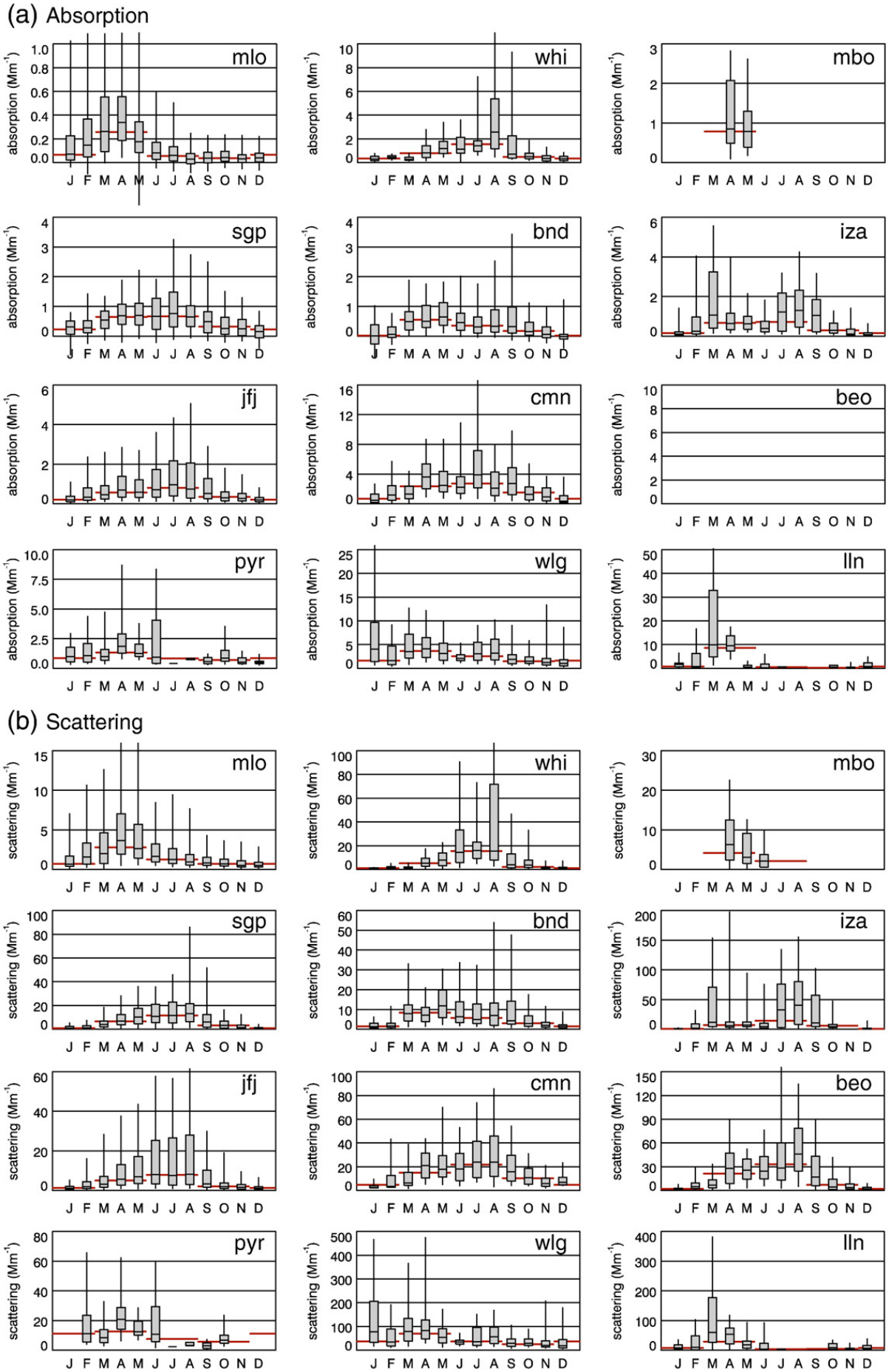

Author's personal copy

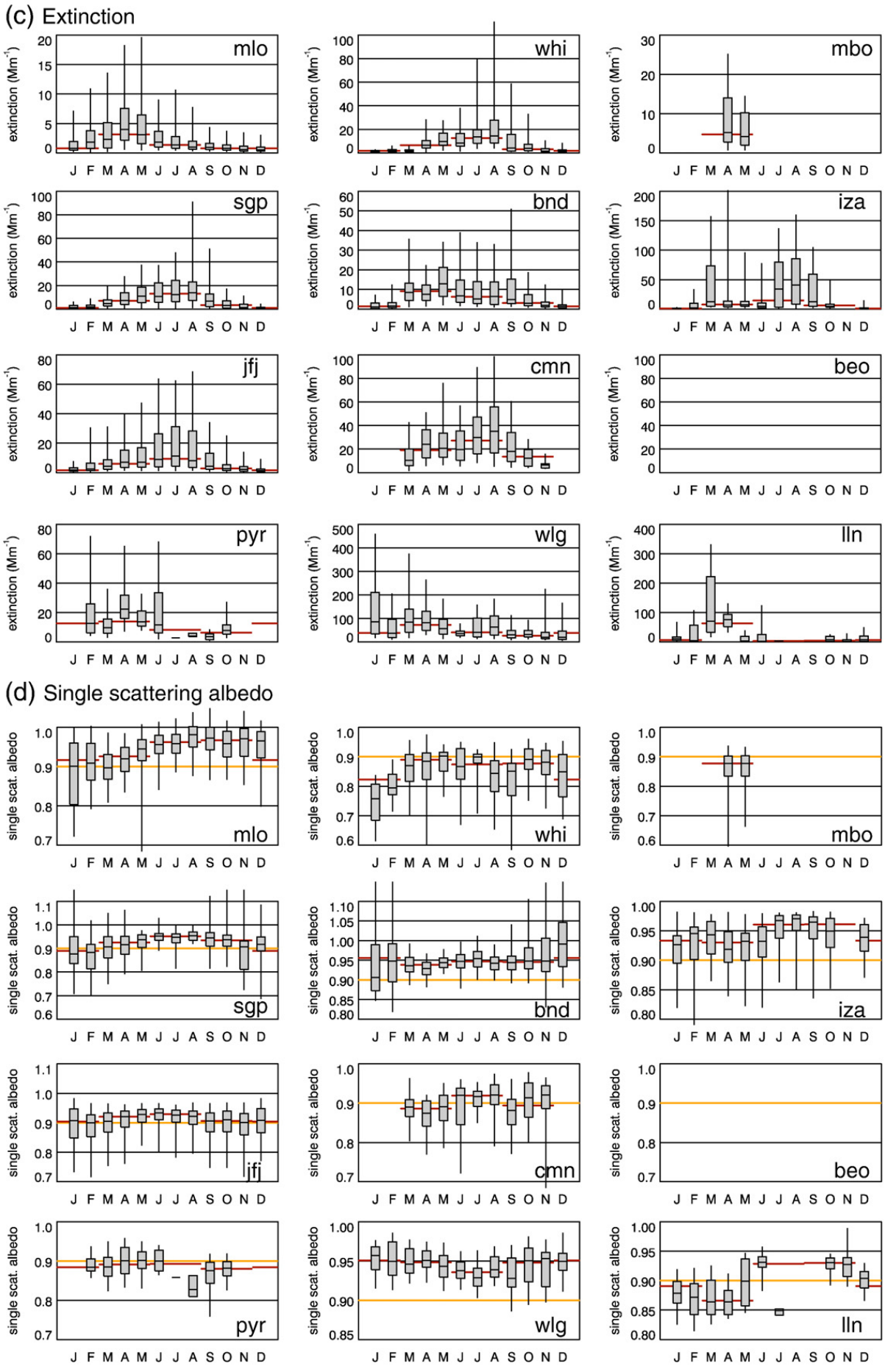

Fig. 4 (*continued*).

Author's personal copy

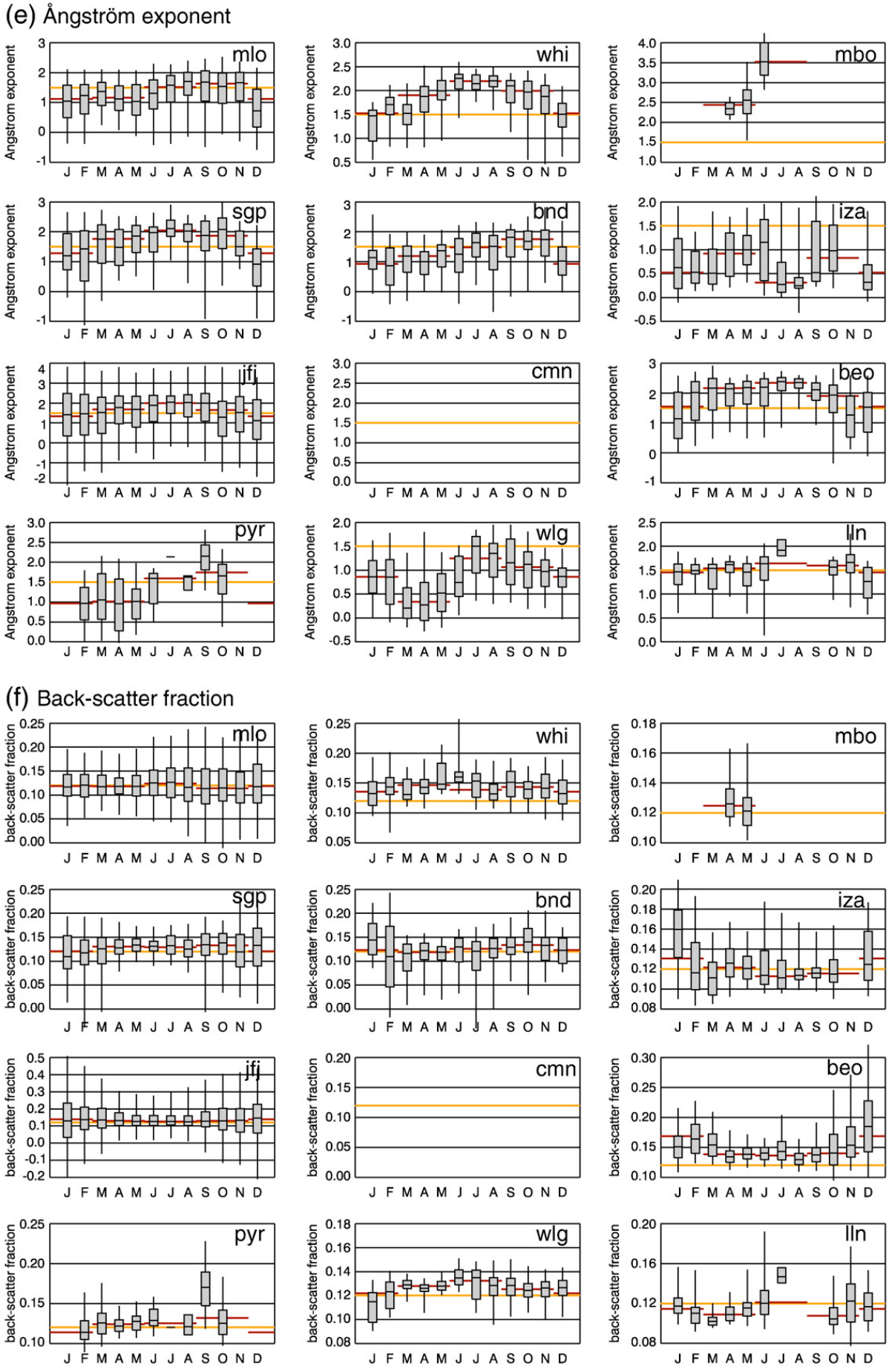

Fig. 4 (*continued*).

Author's personal copy

single scattering albedo values are observed in the summer corresponding to influence from urban regions to the east (Kivekas et al., 2009). The median single scattering albedo value at most sites for most months is in the range 0.90 ± 0.05 although in January the single scattering albedo at WHI has a median value of 0.75. The seasonal cycle in single scattering albedo can be related to known patterns in aerosol transport to the sites. Low single scattering albedo values occur at LLN during the springtime which is when the site is most strongly impacted by biomass burning (Chi et al., 2010, Lin et al., 2010). At WHI low single scattering albedo values occur in both the wintertime and in the summertime. Potential reasons for the low wintertime values are as listed above, while the low summertime values are likely due to forest fire smoke (Mckendry et al., 2010, Gallagher et al., 2011). These monthly climatologies of single scattering albedo demonstrate the relevance of long-term measurements; a short-term field campaign would provide little indication of the large variation in single scattering albedo occurring on a monthly/seasonal basis. Again, it should be noted that these single scattering albedo values represent dry aerosol particles. As the scattering coefficient will respond more strongly to an enhancement in relative humidity than the absorption coefficient (Nessler et al., 2005), the ambient single scattering albedo values are expected to be higher.

3.2.3. Ångström exponent

There is not a consistent seasonal pattern in the Ångström exponent (Fig. 4e) among all the sites, likely due to a combination of differing sources and transport timing. Several locations (WHI, SGP, JFJ, BEO) have lower Ångström exponent values during winter and higher values in late summer and early fall, while at BND the Ångström exponent peaks in late fall. At PYR and WLG the Ångström exponent values are lowest in the spring and highest in the autumn. The annual cycle at WLG is particularly striking; the dramatically lower å values during spring show the strong dust influence at this site. There is a peak in Ångström exponent in September at PYR coinciding with a peak in the backscatter fraction (Fig. 4f). This suggests an increase in smaller particles at the tail end of the monsoon season at PYR, possibly as a result of changed source emissions, circulation or both with the onset of dryer, colder weather. At IZA the months that typically have stronger Saharan dust incursions (February, March, July, August, September) have lower median Ångström exponents than at other times of year. MLO and WHI are, at times, influenced by springtime Asian dust transport (e.g., Bodhaine, 1983; Leaitch et al., 2009). However, there are annual differences in the frequency, intensity and timing of dust events, and the dust is often mixed with pollution (Perry et al., 1999). These factors may explain the lack of a strong springtime dust signal (low Ångström exponent) at these two sites. Another reason the WHI optical data may not show a strong dust signal is that, a springtime field campaign at the site suggested that dust aerosol was primarily found in 2–5 μm particles (e.g., Leaitch et al., 2009), but the optical instruments deployed at WHI have 2.5 μm size cut which would minimize the dust influence on Ångström exponent. Because aerosol extinction tends to be dominated by the scattering contribution for the sites studied here (single scattering albedo typically greater than 0.85), the scattering Ångström exponent is a reasonable surrogate for the extinction Ångström exponent.

3.2.4. Backscatter fraction

There is a narrow range of observed monthly median FT backscatter fraction values, with median values typically near 0.12 ± 0.02 (Fig. 4f). This range in backscatter fraction corresponds to asymmetry parameter values in the range 0.61 ± 0.05 (calculated from Eq. 5). Many sites show very little change in the median backscatter values (MLO, SGP, BND, JFJ, WLG and LLN) throughout the year. At MLO and JFJ the median value of the backscatter fraction is consistent throughout the year. Measurement noise is larger during the cleaner winter months, resulting in the larger range of backscatter fraction displayed in the box-whisker plots. At IZA and BEO the aerosol particles have higher median backscatter fraction in the winter suggesting a larger contribution from small accumulation mode aerosol particles, perhaps due to increased wintertime cloud processing of the size distribution. At IZA the wintertime aerosol size distribution is influenced by downward transport from the mid- and upper troposphere shifting the size distribution to smaller particles (Rodríquez et al., 2009; Raes et al., 1997). BEO also experiences upper atmosphere subsidence in the winter (Nojarov et al., 2009). WHI sees the opposite pattern with an increase in backscatter fraction observed in the spring/summer — this can likely be attributed to enhanced biogenic emissions and, in the summer, forest fire influence (Takahama et al., 2011). Seasonal cycles in backscatter fraction at MBO, PYR and LLN are difficult to interpret due to months with missing data. At LLN the lowest values of backscatter fraction occur in March at the peak of the biomass burning transport to the site. This suggests that the biomass aerosol is dominated by mid- to large diameter accumulation mode particles. For the monthly backscatter fraction climatologies in Fig. 4f there is not a distinct pattern that can be associated with known source temporal patterns, hence it is difficult to relate the changes in backscatter fraction to a specific aerosol type.

3.3. Comparison with satellite measurements

The observations presented here are sufficient to characterize the optical properties of aerosol particles at specific locations and they can be used to determine those parameters that are difficult to obtain from remote sensing measurements (e.g., single scattering albedo, backscatter coefficient, etc. (Anderson et al., 2005)). However Figs. 3 and 4 have shown that there are significant differences in aerosol optical properties in terms of seasonality, amount and nature, even at sites that are relatively close to each other (e.g., SGP and BND or JFJ and CMN). This current analysis makes it obvious there are gaps in the global and regional characterization of aerosol properties because each of the twelve sites included here only provides information at a single point in space. The global coverage delivered by satellite measurements should help fill these gaps. Here we present a comparison of in-situ aerosol extinction with that derived from satellite measurements. The satellite observations represent ambient conditions, but the in-situ data are reported at STP and low RH. As discussed previously, while humidity differences would suggest the satellite extinction measurements should be higher than the in-situ measurements (depending on

Author's personal copy

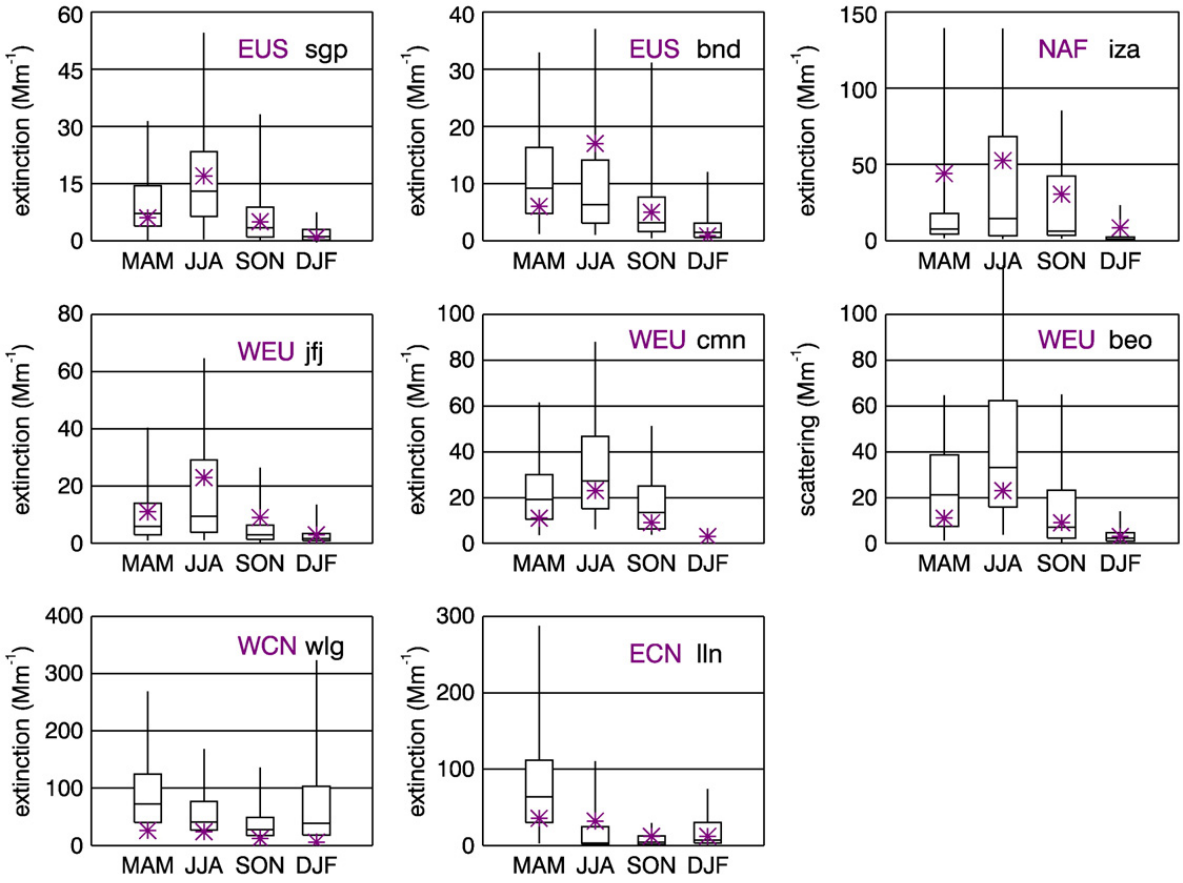

Fig. 5. Comparison of average seasonal CALIPSO ambient extinction values at 3 km (purple) 532 nm with seasonal in-situ extinction (at 550 nm, low RH and STP). Box-whiskers show percentiles as described in Fig. 3. CMN at 520 nm, low RH and STP. The BEO plot shows scattering. EUS is eastern US profile; NAF is northern Africa profile; WEU is western Europe profile; WCN is western China profile and ECN is eastern China profile. CALIPSO values come from Yu et al. (2010).

aerosol composition and size), the STP adjustment is of similar magnitude but has the opposite effect. Note: this compensating effect does not apply to single scattering albedo.

The SAGE II (Stratospheric Aerosol and Gas Experiment II) and CALIPSO (Cloud-Aerosol Lidar and Infrared Pathfinder Satellite Observation) satellites provide vertically resolved aerosol extinction profiles. SAGE II was originally designed for observing the stratosphere but with care its measurements can be extended into the upper troposphere (4–6 km asl) (Treffeisen et al., 2006). We can qualitatively compare the SAGE II latitudinally-averaged seasonal values of FT extinction (at 1020 nm) presented by Kent et al. (1998) (their Plate 4c) with the high altitude observatory measurements presented in Fig. 4. Between 30 and 60°N the highest values of SAGE II extinction are observed in the spring. Some of the mountaintop sites (MLO, LLN) are consistent with the SAGE II observations, and also exhibit a springtime extinction peak, but many of the other high altitude sites exhibit broader peaks in extinction encompassing both spring and summer (Fig. 4c). The SAGE II aerosol extinction increases from south to north across the northern hemisphere midlatitudes but the in-situ extinction measurements do not reveal a consistent north–south gradient. The SAGE II observations at 1020 nm are more sensitive to large particles such as dust so one explanation may be that the SAGE extinction observations are heavily weighted by high intensity springtime dust events. The extinction values from SAGE II peak at ~1 Mm^{-1} in spring which is approximately equivalent to 3 Mm^{-1} at 550 nm, assuming an Ångström exponent of 2 (and equivalent to 2.5 Mm^{-1} at 550 nm, assuming an Ångström exponent of 1.5). This is substantially lower than the springtime median, in-situ extinction data which range from ~3 Mm^{-1} at MLO to 70 Mm^{-1} at WLG. Some of the discrepancy between the satellite and in-situ observations can be attributed to differences in measurement technique and data evaluation. The SAGE measurements presented by Kent et al. (1998) represent the extinction at altitudes between 6 km and the tropopause, which is significantly higher than most of the sites included here. Mattis et al. (2008) use lidar data taken over Leipzig to show that FT extinction values above 5 km are a factor of 2 lower than the FT extinction measured at altitudes below 5 km. The SAGE II cloud-screening algorithm has also been shown to misidentify high aerosol concentrations as clouds. There is also a temporal mismatching between the SAGE II measurements (1979–1998) and the in-situ observations presented here, many of which began after 2005. This comparison of in-situ and SAGE II extinction suggests that the latitudinally-averaged SAGE II extinction observations in Kent et al. (1998) are not representative of the in-situ FT extinction obtained from the high altitude platforms in this study.

The CALIOP lidar on-board the CALIPSO satellite measures aerosol extinction at 532 nm with good vertical resolution (30 m in the low and middle atmosphere (Yu et al., 2010))

Author's personal copy

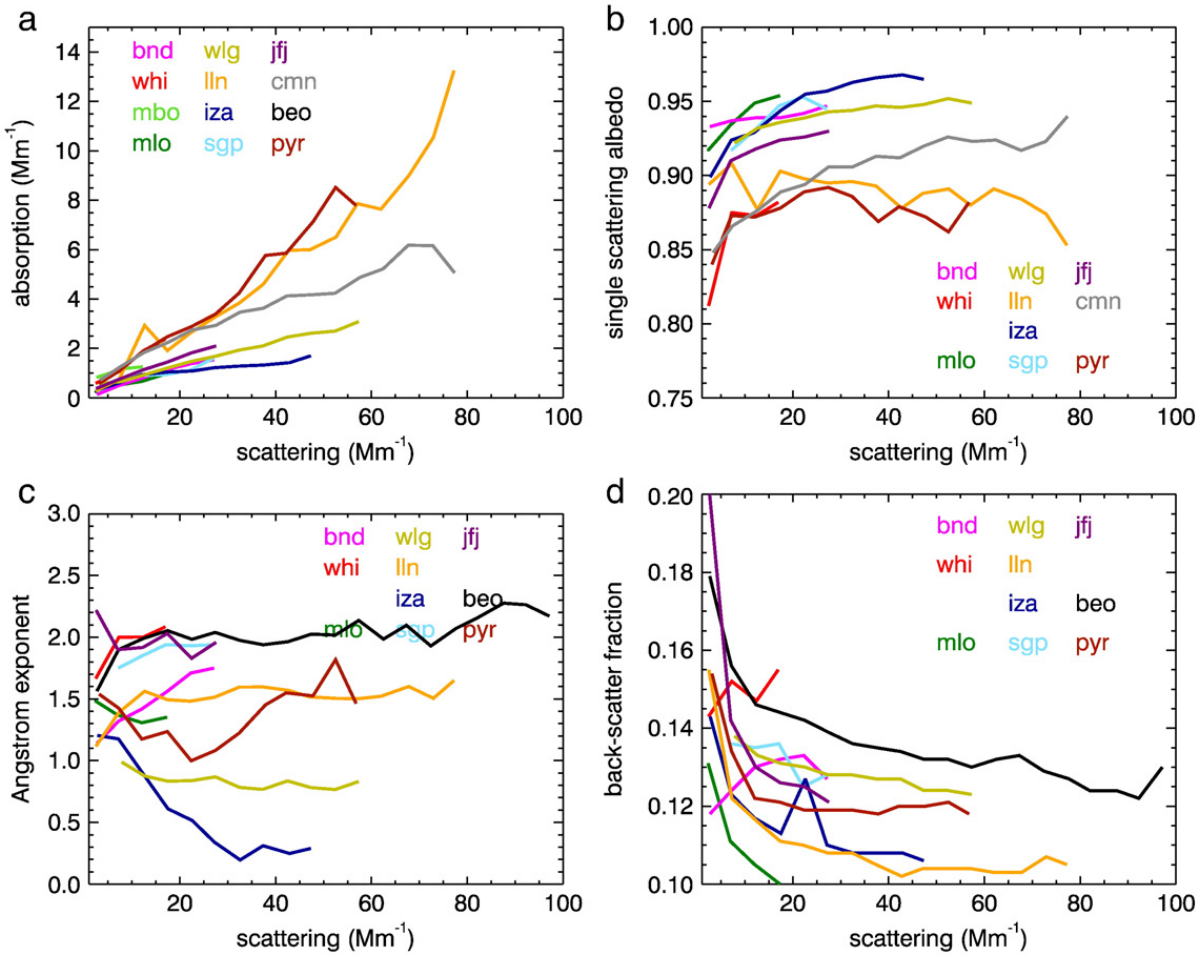

Fig. 6. Systematic variability of various mean aerosol optical properties with aerosol light scattering: (a) light absorption, (b) single scattering albedo, (c) Ångström exponent, (d) backscatter fraction. Single scattering albedo, Ångström exponent and backscatter fraction are calculated with the constraint light scattering >1 Mm^{-1} to minimize noise caused by taking ratio of two small numbers. CMN scattering is at 520 nm, at all other sites scattering is at 550 nm.

down into the boundary layer (Winker et al., 2007). Thus the CALIPSO data are more suitable to compare with the high altitude in-situ measurements. Yu et al. (2010) present seasonal average extinction profiles based on CALIPSO data from June 2006 to November 2007 for several regions. Fig. 5 shows seasonal variability of in-situ aerosol light extinction for 8 sites along with the seasonal extinction at 3 km altitude for the appropriate overlap region from Yu et al. (2010). This figure represents a comparison of low relative humidity, in-situ extinction measurements (at STP and at 550 nm) to average extinction measurements from CALIPSO (ambient RH, T, P and at 532 nm).

In general the comparisons suggest strong similarities in terms of seasonal cycle and aerosol amount. For the eastern US region comparison with SGP and the western Europe region comparisons with JFJ, CMN and BEO the satellite extinction values have the same seasonal pattern and are quite similar in magnitude to the in-situ extinction. The comparison between the CALIPSO eastern U.S. region and in-situ data from SGP is excellent. For BND, also compared with the CALIPSO eastern U.S. region, the comparison is not as good as for SGP — the values of extinction are quite similar for both in-situ and CALIPSO measurements but the seasonal in-situ extinction measurements peak in spring while CALIPSO measurements for the eastern US indicate a summertime extinction maximum. The springtime values for IZA and the CALIPSO northern Africa region exhibit the largest discrepancy of any of the comparisons, with CALIPSO being much higher than the in-situ measurements. There are two possible explanations for this difference. This could be due to stronger outflow from Africa in spring 2007 compared to the 2008–2009 time period covered by the IZA measurements. It is also possible that the northern Africa region is not representative of the aerosol sampled at IZA. The comparison between WLG and CALIPSO observations over western China suggests that CALIPSO underestimates aerosol extinction in this region. As with IZA, the CALIPSO results are regional averages that may not be representative of a single point and temporal differences in the two measurement periods may also play a role in the discrepancy. Yu et al. (2010) also suggest that CALIPSO may underestimate extinction due to dust. The results presented in Fig. 5 are obviously not an exhaustive comparison but it suggests the potential for CALIPSO to provide global free tropospheric aerosol extinction values and provides validation for the lidar ratio that NASA uses to derive extinction from the 180-degree backscatter.

3.4. Systematic relationships among aerosol properties

A better understanding of systematic variability among aerosol properties can help to constrain model parameterizations of

Author's personal copy

those aerosol properties and also reduce uncertainties in algorithms for deriving aerosol optical properties from remotely sensed data (Delene and Ogren, 2002). Spatial and temporal resolution in models can make it difficult to directly compare absolute values of absorption and scattering from in-situ point measurements with model predictions, however, comparison of measured and modeled systematic variability may help indicate whether models are properly incorporating emissions, transport and atmospheric processing (e.g., cloud scavenging) into their computations. Fig. 6 demonstrates how several aerosol properties (light absorption, Ångström exponent, single scattering albedo, and backscatter fraction) vary with aerosol loading (as represented by light scattering). The median aerosol optical properties were calculated over 5 Mm^{-1} light scattering intervals. The standard error (SE = standard deviation of sample/square root of number of points in sample) was calculated for each scattering bin for each of the parameters plotted. Fig. 6 only includes points where the SE was less than ~2% of a typical value of the parameters plotted on the y-axis, i.e., for single scattering albedo the SE<0.02, for backscatter fraction SE<0.002, and for Ångström exponent SE<0.04. This choice ensured that the systematic variability depicted is representative of the data set as a whole. Data from MBO is only shown on Fig. 6a, the SE for the MBO intensive parameters was too large due to low numbers of data points.

3.4.1. Light absorption vs. light scattering

Aerosol light absorption and scattering vary approximately linearly, with light absorption generally increasing with increasing light scattering as would be expected from Fig. 4ab. The slope of the relationship between light scattering and absorption differs amongst the stations and is equal to $1/\omega_o - 1$. At lower aerosol loadings (σ_{sp}<20 Mm^{-1}) the lines for many of the sites overlap. This indicates similar proportions of scattering and absorbing aerosol across those sites during clean periods. The IZA measurements, which are dominated by dust aerosol at high aerosol loading (Maring et al., 2000), tend to have a lower slope than the other sites. PYR and LLN, two sites where high aerosol loading coincides with the presence of pollution and/or biomass burning plumes have larger slopes. PYR is also influenced by dust transport, but the relationship between Ångström exponent and light scattering (Fig. 6c) suggests that the dust events are more likely to occur during time periods of lower aerosol loading. This is consistent with observations of aerosol mass loading at PYR — Table 1 in Marinoni et al. (2010) shows relatively more coarse aerosol during lower mass loading periods. The slope for the absorption-scattering relationship at CMN lies in-between those of PYR and LLN and the other 10 stations. This could reflect that both dust and smoke plumes are transported to CMN and both types of plumes correspond to high aerosol loading. The larger slopes for PYR, LLN and CMN are reflected in the single scattering albedo plot (Fig. 6b).

3.4.2. Single scattering albedo vs. light scattering

Fig. 6b suggests that, in general, single scattering albedo is lowest at low aerosol loading, and then increases to some approximately constant value as aerosol loading increases. The observation of low values of single scattering albedo at low aerosol loading is consistent with an aerosol mixture in which large scattering aerosol particles have been preferentially removed (e.g., by cloud scavenging and/or deposition), leaving behind a relatively darker aerosol (e.g., Berkowitz et al., 2011; Sellegri et al., 2003, Marcq et al., 2010; Targino et al., 2005). The LLN plot does not follow the pattern of the other stations; at LLN the single scattering albedo is approximately constant for most of the scattering range, but decreases slightly at the highest scattering values. This could be explained if the highest scattering values observed at LLN are associated with transported biomass burning aerosol and/or the highest loadings correspond with the least processed (freshest) biomass plumes. Similarly, comparisons of the aerosol optical properties of local and long range transported biomass smoke at SGP showed that local (fresh) smoke had a lower single scattering albedo than smoke that was transported over several days and ~1000 km distance (Andrews et al., 2004). Reid et al. (2005) present an overview of single scattering albedo measured in various ways (in-situ, remote sensing) that suggests single scattering albedo will increase as the smoke aerosol ages. They suggest two mechanisms for this increase (1) transformation of the aerosol by

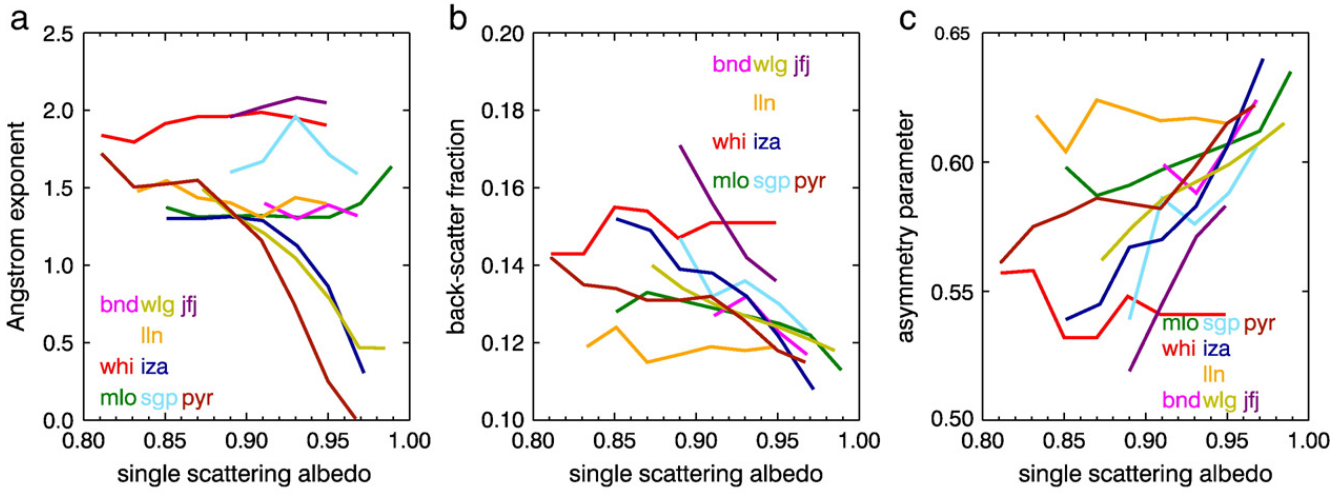

Fig. 7. Systematic variability as a function of single scattering albedo (a) single scattering albedo vs. Ångström exponent (b) single scattering albedo vs. backscatter fraction (c) single scattering albedo vs. asymmetry parameter. Single scattering albedo, Ångström exponent and backscatter fraction are calculated with the constraint light scattering >1 Mm^{-1} to minimize noise caused by taking ratio of two small numbers.

Author's personal copy

Table 3
Constants for TOA forcing efficiency calculation.
From Haywood and Shine (1995).

Parameter	value
D (fractional day length)	0.5
S_o (solar constant)	1370 W m^{-2}
T_{at} (atmospheric transmission)	0.76
A_c (cloud fraction)	0.6
R_s (surface reflectance)	0.15

in of less absorbing aerosol from other sources. Such an effect may also occur for pollution plumes during transport. Fischer et al. (2010) compare single scattering albedo values observed in aged Asian plumes at MBO. They show that for Asian air masses transported across the Pacific Ocean, the single scattering albedo increases with age due to transformation of the aerosol by condensation and coagulation during transport.

3.4.3. Ångström exponent vs. light scattering

The Ångström exponent is between 1 and 1.7 at most of the sites during periods of very low loading (σ_{sp}<10 Mm^{-1}). The Ångström exponent values reported for MBO are higher due to the 1 μm impactor upstream of the nephelometer. Fig. 6c shows that the Ångström exponent can increase or decrease as aerosol loading increases depending on the site. The Ångström exponent at dust-influenced sites (IZA and WLG) decreases with aerosol loading indicating that at these sites the highest aerosol loads are due to strong dust events. A similar decrease in Ångström exponent with increased loading can also be seen at marine sites (Delene and Ogren, 2002), however a marine influence is unlikely to be a major influence for the FT aerosol particles investigated here. The PYR relationship falls between those of IZA and WLG and the rest of the sites, consistent with the influence of both dust and biomass burning at PYR. For the remaining sites, the Ångström exponent increases with loading which one would expect for anthropogenic pollution or biomass burning plumes (Toledano et al., 2007).

The relationship between Ångström exponent and scattering depicted in Fig. 6c can be compared with similar relationships developed from spectral column measurements of aerosol optical depth (AOD) and Ångström exponent at various AERONET sites. The variability in aerosol loading with Ångström exponent can be attributed to changes in aerosol type due to changes in source or changes in contribution of a source (Eck et al., 1999; Dubovik et al., 2002; Toledano et al., 2007). This is most clearly illustrated by Toledano et al. (2007) who show how the Ångström exponent and AOD relationship vary as a function of five different aerosol types sampled at the El Arenosillo station in southwestern Spain. They show (in their Fig. 11) that desert dust events detected at El Arenosillo are represented by low Ångström exponent and high AOD, while biomass burning and continental aerosol particles have high Ångström exponent values along with high AOD. This is consistent with the relationship between Ångström exponent and aerosol light scattering presented for the in-situ data in this study.

3.4.4. Backscatter fraction vs. light scattering

Similar to what was presented in Delene and Ogren (2002) the backscatter fraction tends to decrease with aerosol loading at most high altitude sites (Fig. 6d). BND and WHI are the only sites that display the opposite relationship: backscatter fraction increases with increasing aerosol light scattering. The higher values of backscatter fraction at lower aerosol loading indicate a greater contribution from smaller accumulation mode particles. This would be consistent with the preferential removal of large particles by cloud scavenging and or depositional losses during transport of the aerosol particles to the site, shifting the size distribution to the small end of the accumulation mode. Alternatively, new particle formation (which occurs within clean air masses) followed by condensation/coagulation could generate small but eventually optically active particles.

3.4.5. Ångström exponent and asymmetry parameter vs. single scattering albedo

The previous sections show that the relationships between intensive aerosol properties and aerosol loading can be related to aerosol type and atmospheric processing such as cloud scavenging. The relationships among the intensive properties can also provide information about the size and composition characteristics of the aerosol. Fig. 7 shows the systematic variability of Ångström exponent, backscatter fraction and asymmetry parameter with single scattering albedo for the sites studied here. Again, only points with low standard error are plotted. The median aerosol optical properties were calculated over 0.02 single scattering albedo intervals.

In Fig. 7a most of the sites show little variability of Ångström exponent over the range of single scattering albedo. In contrast, the Ångström exponents at the three dust-influenced sites (PYR, WLG and IZA) vary in a similar fashion; the Ångström exponent decreases as single scattering albedo increases. This suggests that the absolute increase in light scattering is larger than that of light absorption in the dust sampled at these sites. Fischer et al. (2010) present similar results for MBO (their Fig. 5c): Asian plumes containing dust were characterized by both high single scattering albedo and low Ångström exponent values compared to Asian aerosol plumes without a large contribution from dust. Collaud Coen et al. (2004) indicate that this type of relationship (low å, high ω_o) can be also used to identify dust events at JFJ (their Figs. 1 and 3) although they note that the wavelength dependence of single scattering albedo is the definitive way to identify a dust event. At lower single scattering albedo values (ω_o<0.9), the LLN and PYR lines show the tendency of Ångström exponent to increase with decreasing single scattering albedo. LLN and PYR are impacted by smoke from bio-mass burning smoke and this observation is

Fig. 8. (a) Free troposphere radiative forcing efficiency. Box-whiskers show percentiles as described in Fig. 3. RFE is calculated with the constraint light scattering >1 Mm^{-1} to minimize noise caused by taking ratio of two small numbers. (b) Monthly variation of FT RFE. Box-whiskers show percentiles as described in Fig. 3. RFE is calculated with the constraint light scattering >1 Mm^{-1} to minimize noise caused by taking the ratio of two small numbers. The purple line represents the RFE_{clim} calculated when the site-specific climatological single scattering albedo and FT backscatter fraction from Fig. 3d and f are used. (c) RFE as function of scattering coefficient in the FT. RFE is calculated with the constraint light scattering >1 Mm^{-1} to minimize noise caused by taking the ratio of two small numbers.

Author's personal copy

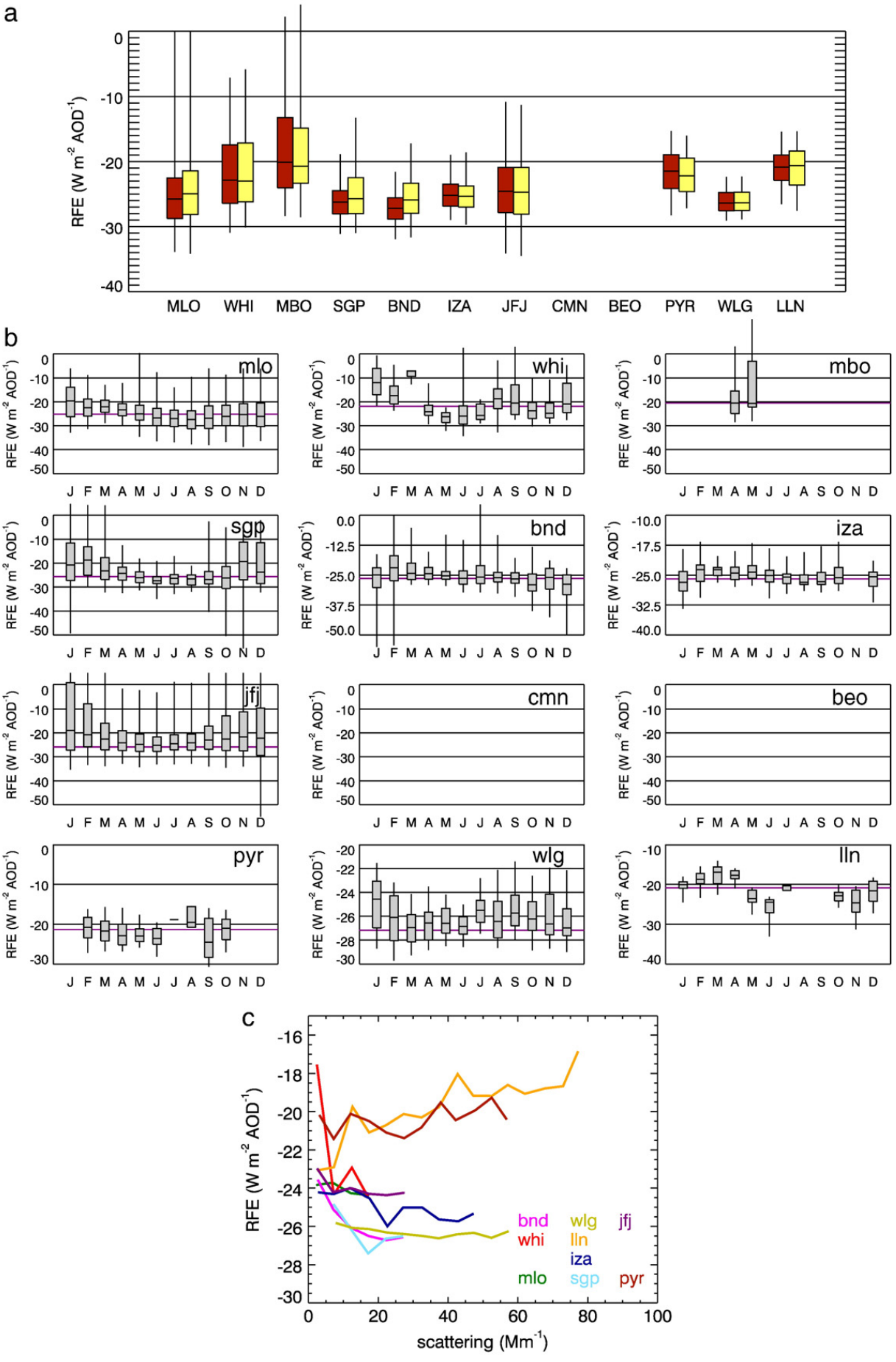

Author's personal copy

consistent with that reported by Reid et al. (1999) for smoke in Brazil.

Fig. 7bc shows the systematic variation of backscatter fraction and asymmetry parameter with single scattering albedo for FT aerosol particles for the sites in this study. The asymmetry parameter is related to backscatter fraction by Eq. (5). The asymmetry parameter and backscatter fraction are two simple surrogates for the aerosol phase function and estimates of aerosol radiative forcing efficiency require single scattering albedo plus some representation of the angular scattering of light. Andrews et al. (2006) discuss different methods for calculating radiative forcing efficiency depending on what in-situ measurements are available. At most sites, the asymmetry parameter increases with single scattering albedo while backscatter fraction decreases. Andrews et al. (2006) presented a similar systematic variation (in their Fig. 5) between these two parameters for the SGP surface site and airplane measurements (not FT). They suggest one explanation for the observed relationship between single scattering albedo and backscatter fraction (or asymmetry parameter) is preferential cloud scavenging of larger, primarily scattering aerosol. Data from remote sensing instruments show similar variability between column average asymmetry parameter and single scattering albedo (Liu et al., 2008a). WHI and LLN are the exceptions to this relationship — the aerosol particles at these two sites have the highest (LLN) and lowest (WHI) asymmetry parameter and asymmetry parameter is relatively constant across the range of single scattering albedo for both sites.

3.5. Radiative forcing efficiency of free troposphere aerosol at low RH conditions

Haywood and Shine (1995) present an equation (Eq. (3) in their paper):

$$\frac{\Delta F}{AOD} = -DS_o T_{at}^2 (1-A_c)\omega_o \beta \left\{ (1-R_s)^2 \cdot \left(\frac{2R_s}{\beta}\right)\left[\left(\frac{1}{\omega_o}\right)-1\right]\right\} \quad (7)$$

to calculate global mean, annually averaged, top of the atmosphere aerosol forcing (ΔF) if ω_o, β, a function of backscatter fraction: ($\beta = 0.0817 + 1.8495b - 2.9682b^2$) and aerosol optical depth (AOD) are known. The ratio of ΔF/AOD is known as the aerosol radiative forcing efficiency (RFE). RFE depends only on the nature of the aerosol (the right side of Eq. (7)) rather than the amount (Sheridan and Ogren, 1999), i.e., AOD is not needed for the calculation of RFE. Simplifying assumptions (e.g., no spectral dependence of aerosol optical properties, changes in surface albedo, etc.) mean that the calculation is really just a zero-order estimate of radiative flux changes. Table 3 provides the values assumed here for the constants in the RFE equation. By using the same values for each of these parameters (D, S_o, T_{at}, A_c, and R_s), and varying only single scattering albedo and backscatter fraction the intrinsic radiative forcing efficiency of the dry aerosols due to changes in these properties can be compared. The climatology and seasonal variation of RFE is presented first and then the RFE calculation is used to explore the sensitivity of aerosol forcing to variations in single scattering albedo and backscatter fraction. It should be stressed that the values of RFE presented here do not represent the actual top of atmosphere radiative forcing efficiency — those will be quite different for each site due to differences in relative humidity, solar angle, surface albedo (i.e., snow versus lava rock), etc.

Fig. 8a presents a climatology of calculated top of atmosphere RFE for ten sites in this study for all data available and for data identified as FT using the time of day restriction. Backscatter fraction is not available for CMN and single scattering albedo is not available for BEO so RFE was not calculated for these two sites. Despite significant variability in the aerosol optical properties observed among the sites (Fig. 3), the median RFE falls between −20 and −30 W m^{-2} AOD^{-1} for both 'all data' and 'FT data'. The four sites with the lowest single scattering albedo (WHI, MBO, PYR and LLN) have the least negative RFE, i.e., their aerosol is slightly less cooling than the sites with more negative RFE. At some sites the RFE increases in the FT compared to that calculated for 'all data' while at others there is little change or a slight decrease. The sites with the biggest increases in RFE between 'all data' and 'FT data' are MLO, SGP and BND. At MLO and SGP this shift appears to be controlled by differences in single scattering albedo for 'all data' and 'FT data' (Fig. 3d), while at BND the shift is controlled by a change in backscatter fraction (Fig. 3f).

Fig. 8b shows the monthly variability of RFE and demonstrates the need for simultaneous measurements of backscatter fraction and single-scattering albedo for quantifying aerosol direct radiative forcing. For example, at IZA the aerosol single scattering albedo is relatively constant regardless of season but backscatter fraction is high in the winter and lower at other times of year. The monthly values of RFE at IZA are lower (more cooling) when backscatter fraction is higher, i.e., when more sunlight is reflected back to space. In contrast, the aerosol at MLO undergoes seasonal changes in single scattering albedo but the backscatter fraction is relatively constant. The resulting RFE is highest (more warming) in the winter months when the single scattering albedo is lower. At the other sites, where single scattering albedo and backscatter fraction co-vary, both parameters play a role in controlling the RFE. Biomass burning plumes impact LLN in the spring and WHI in summer causing lower single scattering albedo values which are reflected in higher (more warming) RFE in those months at those stations.

To investigate how well the assumption of static values for single scattering albedo and backscatter fraction can represent the observed temporal variability in RFE, the calculated monthly RFE values are compared with RFE_{clim} (calculated using site-specific climatological medians of single scattering albedo (from Fig. 3d) and backscatter fraction (from Fig. 3f)). RFE_{clim} is represented in Fig. 8b by a purple line. At some sites (IZA, WLG), the monthly RFE values are within 10% of RFE_{clim}, suggesting site-specific climatological values may reasonably be used to calculate forcing at these sites. At MBO the median values of RFE and RFE_{clim} are virtually on top of each other, however RFE_{clim} is based on only two months of data and may not represent measurements outside that limited time period. At other sites, the monthly median values of RFE can be quite different (10–35%) from RFE_{clim}. The biggest one month discrepancy is at WHI where the March RFE value (~7 W m^{-2} AOD^{-1}) is a factor of 3 different than the RFE_{clim} value of ~−22 W m^{-2} AOD^{-1}. This comparison indicates the importance of using appropriate values of single scattering albedo and backscatter fraction and understanding that

Author's personal copy

large uncertainties in RFE and hence aerosol forcing may ensue when the variability in single scattering albedo and backscatter fraction are not considered. At most sites the differences between RFE_{clim} and the monthly median RFE tend to be larger for lower aerosol loading. This is consistent with the observation that we see the most variability in single scattering albedo and backscatter fraction at low loading conditions (Section 3.1). We also see the widest range of single scattering albedo and backscatter fraction values among sites at low loading (e.g. Fig. 6bd).

Fig. 8c depicts the systematic variability between aerosol light scattering and RFE. When the light scattering coefficient is greater than ~10 Mm^{-1} the RFE is relatively constant (less than ± 1 W m^{-2} AOD^{-1} variability) for all the sites except LLN. A constant RFE does not mean that the absolute aerosol radiative forcing is constant — aerosol radiative forcing changes with aerosol loading — it just suggests that the intrinsic nature of the aerosol will not significantly affect the calculation of RFE. At LLN the RFE increases by ~6 W m^{-2} AOD^{-1} (i.e., relatively more warming) as the light scattering coefficient increases from 0 to ~80 Mm^{-1}. The high values of scattering at LLN tend to occur in the spring due to transport of smoke from regional biomass burning in the region and the increase in RFE is consistent with a more strongly absorbing aerosol. For low aerosol loading (σ_{sp}<10 Mm^{-1}) the RFE appears to be slightly less negative (i.e., relatively more warming) than for higher aerosol loading conditions at all sites but LLN. This is consistent with the picture of smaller, darker aerosol at low aerosol loadings depicted in Fig. 6. The WHI aerosol has the highest RFE at low aerosol loading — this is likely associated with the low wintertime single scattering albedo values at the WHI discussed in Section 3.1.2. The variation of RFE with aerosol amount ranges from quite low (<0.5 W m^{-2} AOD^{-1}) at JFJ up to ~6 W m^{-2} AOD^{-1} at WHI and LLN. This latter value is quite a bit more variable than the ~± 1 W m^{-2} AOD^{-1} that was observed for the four sites studied by Delene and Ogren (2002). Based on the low variability in RFE over the wide range of aerosol loading at the sites they studied (0–140 Mm^{-1}), Delene and Ogren (2002) hypothesized that the amount of aerosol is of primary importance in direct radiative forcing calculations while the value of the intensive aerosol optical properties (single scattering albedo and backscatter fraction) is of secondary importance. With the possible exception of measurements at LLN and WHI, our results are consistent with the hypothesis presented by Delene and Ogren (2002).

4. Conclusions

An overview of free troposphere (FT) aerosol optical properties determined from high altitude in-situ measurements at locations across the northern hemisphere has been presented in this paper. Time of day was used to identify periods of FT air, with the caveat that this simple approach is likely to include boundary layer air at certain locations and during specific synoptic conditions. There is significant variability in aerosol optical properties in terms of aerosol loading (light absorption, scattering and extinction) and intensive properties (single scattering albedo, Ångström exponent and backscatter fraction) among the 12 sites. Aerosol loading generally increased on a west to east gradient where the western-most site was Mauna Loa (MLO) in Hawaii and the eastern-most site was Mount Lulin (LLN) in Taiwan. Differences in the intensive properties clearly showed the influence of different sources/aerosol types on the different sites.

There were clear seasonal cycles in aerosol loading with the peak occurring in spring (LLN and MLO) or spring/summer (all the other sites). In-situ extinction values from the European observatories (Jungfraujoch (JFJ), Monte Cimone (CMN), Beo Moussala (BEO)) were in the same range as FT extinction measured by the EARLINET lidar network. The annual cycles for intensive properties were less well-defined and more variable (e.g., depending on the site, the lowest single scattering albedo could occur in spring (LLN), summer (Mount Waliguan (WLG)), fall (Nepal Climate Observatory — Pyramid (PYR)) or winter (MLO)). In general, the changes in intensive property values could be related to known sources and the timing of their maximum impact (e.g., biomass burning transport to LLN and dust transport to Izaña (IZA)).

There were large discrepancies between the in-situ extinction values and averaged SAGE II upper troposphere extinction data. In contrast, comparisons of in-situ aerosol extinction measurements with regional extinction profiles derived from CALIPSO presented in Yu et al. (2010) were in good agreement both in absolute amount and in seasonal cycle. This result suggests that aggregated CALIPSO swaths are likely to provide a relatively accurate global map of FT seasonal aerosol extinction (to the extent that aerosol hygroscopic growth can be assumed to be equal in magnitude but opposite in effect to the STP conditions at which these high altitude aerosol particles were reported). However, in-situ measurements are still crucial for determining other aerosol optical properties in the FT.

Investigation of the systematic variability of aerosol properties as a function both of aerosol loading and of single scattering albedo demonstrated common patterns that could help constrain model estimates of aerosol parameters. Cloud-scavenging during transport was hypothesized as on explanation for the observation that aerosol particles were more absorbing (lower single scattering albedo) and smaller (higher back scatter fraction) at low aerosol loading. The Ångström exponent-light scattering relationship showed different patterns for dust aerosol (Ångström exponent decreases with loading) and pollution/biomass burning aerosol (Ångström exponent increases with loading) similar to Ångström exponent-aerosol optical depth relationships derived from AERONET sunphotometer measurements. These systematic variations may be useful for identifying aerosol type if other information such as aerosol chemistry is unknown. The ability of models to reproduce the systematic variability of aerosol optical properties derived from in-situ measurements may also be a useful way to assess whether models are properly simulating the processing that occurs during atmospheric transport.

Despite large variability in aerosol extensive and intensive properties among the sites, the median values of the top of atmosphere radiative forcing efficiency (RFE = radiative forcing/optical depth) were in a narrow range between −30 to −20 W m^{-2} AOD^{-1} at all the sites. Seasonal variations in RFE were related to changes in single scattering albedo and backscatter fraction. The difference between median monthly RFE and RFE_{clim} calculated using the site-specific climatological median single scattering albedo and backscatter fraction

Author's personal copy

were in the 10–35% range for most sites. These differences tended to be larger at low aerosol loading consistent with the observation that these aerosol optical properties spanned a larger range of values at cleaner conditions. At most sites the radiative forcing efficiency at low aerosol loading (light scattering $<10\ Mm^{-1}$) was slightly less negative (more warming) than at higher aerosol. Consistent with the analysis by Delene and Ogren (2002) the aerosol loading was typically more important for direct aerosol radiative forcing of climate than the intensive properties (single scattering albedo, backscatter fraction) of the aerosol particles.

Acknowledgments

We gratefully acknowledge the NOAA observatory staff at MLO, the pilots of the SGP and BND airplanes and folks at Greenwood Aviation in Ponca City, OK.

Co-operation and support from the Environmental Management group of Whistler–Blackcomb is gratefully acknowledged. We thank the site operators, Juniper Buller and Anton Horvath, the maintenance staff, lift operators and members of ski patrol. We also thank Dave Halpin for technical support.

Support for the Mount Bachelor Observatory was provided by the National Science Foundation under grant ATM-0724327. Emily V. Fischer was supported by a Department of Energy Graduate Research Environmental Fellowship.

Measurements at Izaña were made within the project GRACCIE (CSD2007-00067; Ministry of Science and Innovation of Spain).

We thank the International Foundation High Altitude Research Stations Jungfraujoch and Gornergrat (HFSJG), which made it possible to carry out the experiments at the High Altitude Research Station at the Jungfraujoch. This work was supported by MeteoSwiss within the Swiss program of the Global Atmosphere Watch (GAW) of the World Meteorological Organization as well as the EU FP6 project EUSAAR.

Monte Cimone data presented here benefited from measurements performed within the European Commission funded FP6-EUSAAR Integrated Infrastructure Initiative.

Measurements of optical properties of aerosols at BEO "Mousala" began in the framework of the FP6 EUSAAR project and thanks to this project. NOAA/ESRL Global Monitoring Division is a source of methodical help and software support which is highly appreciated. Special gratitude deserves the technical staff of BEO (Bobi, Plamen Miki, Zahi) who work in very severe environmental conditions. Thanks to all the people who feel BEO "Moussala" close to their hearts and help it to work day after day.

Measurements at PYR were carried out in the framework of the UNEP — ABC (Atmospheric Brown Clouds) and EvK2CNR — SHARE (Stations at High Altitude for Research on the Environment) projects.

This work at Mt. Waliguan was supported by The China International Science and Technology Cooperation Project (2009DFA22800), National Basic Research Program of China (2011CB403401), and key project of CAMS (2010Z002). The authors would also like to thank the staff of China GAW Baseline Observatory (Mt. Waliguan) for operating and maintaining the instruments at the station.

The dedication of the staff (Ferret, Eric and Josh) at Lulin Mountain is much appreciated.

References

Alastuey, A., Querol, X., Castillo, S., Escudero, M., Avila, A., Cuevas, E., Torres, C., Romero, P.M., Exposito, F., Garcia, O., Diaz, J.P., Dingenen, R.V., Putaud, J.P., 2005. Characterisation of TSP and PM2.5 at Izaña and Sta. Cruz de Tenerife (Canary Islands, Spain) during a Saharan dust episode (July 2002). Atmos. Environ. 39 (26), 4715–4728.

Anderson, T.L., Ogren, J.A., 1998. Determining aerosol radiative properties using the TSI 3563 integrating nephelometer. Aerosol Sci. Tech. 29 (1), 57–69.

Anderson, T.L., et al., 2005. An "A-Train" strategy for quantifying direct climate forcing by anthropogenic aerosols. Bull. Amer. Meteor. Soc. 86, 1795–1809.

Andrews, E., Ogren, J.A., Sheridan, P.J., Ferrare, R., 2004. Vertical properties of aerosol optical properties at the ARM Southern Great Plains CART site. J. Geophys. Res. 109 (D6) Art. No. D06208.

Andrews, E., Sheridan, P.J., Fiebig, M., McComiskey, M., Ogren, J.A., Arnott, P., Covert, D., Elleman, R., Gasparini, R., Collins, D., Jonsson, H., Schmid, B., Wang, J., 2006. Comparison of methods for deriving aerosol asymmetry parameter. J. Geophys. Res. 111. doi:10.1029/2004JD005734.

Angelov, C., Angelov, I., Arsov, T., Archangelova, N., Boyukliiski, A., Damianova, A., Drenska, M., Georgiev, K., Kalapov, I., Nishev, A., Nikolova, N., Penev, I., Sivriev, I., Stamenov, J., Tchorbadjieff, A., Todorov, S., Vachev, B., 2011. "BEO Moussala — a new facility for complex environment studies" sustainable development in mountain regions southeastern Europe, part 2. Springer, pp. 123–139. doi:10.1007/978-94-007-0131-1_11.

Baltensperger, U., Gaggeler, H.W., Jost, D.T., Emmenegger, M., Nageli, W., 1991. Continuous background aerosol monitoring with the Epiphaniometer. Atmos. Environ. 25A, 629–634.

Baltensperger, U., Gaggeler, H.W., Jost, D.T., Lugauer, M., Schwikowski, M., Weingartner, E., Seibert, P., 1997. Aerosol climatology at the high-alpine site Jungfraujoch, Switzerland. J. Geophys. Res. 102, 19,707–19,715.

Barnaba, F., Putaud, J.P., Gruening, C., dell'Acqua, A., Dos Santos, S., 2010. Annual cycle in co-located in situ, total-column, and height-resolved aerosol observations in the Po Valley (Italy): implications for ground-level particulate matter mass concentration estimation from remote sensing. J. Geophys. Res. 115. doi:10.1029/2009JD013002.

Bergstrom, R.W., Russell, P.B., Hignett, P., 2002. Wavelength dependence of the absorption of black carbon particles: predictions and results from the TARFOX experiment and implications for the aerosol single scattering albedo. J. Atmos. Sci. 59 (3), 567–577.

Berkowitz, C., Berg, L.K., Yu, X.-Y., Alexander, M.L., Laskin, A., Xie, Y., Jobson, B.T., Andrews, E., Ogren, J., 2011. A statistical overview of aerosol optical, chemical and physical measurements at a coastal northern California site during the summer of 2005. Atmos. Env. 45, 2559–2568.

Bodhaine, B., 1983. Aerosol measurements at four background sites. J. Geophys. Res. 88, 10,753–10,768.

Bodhaine, B., 1995. Aerosol absorption measurements at Barrow, Mauna Loa and the South Pole. J. Geophys. Res. 100, 8967–8975.

Bonasoni, P., Stohl, A., Cristofanelli, P., Calzolari, F., Colombo, T., Evangelisti, F., 2000. Background ozone variations at Mt. Cimone Station. Atmos. Environ. 34, 5183–5189.

Bonasoni, P., Laj, P., Angelini, F., Arduini, J., Bonafè, U., Calzolari, F., Cristofanelli, P., Decesari, S., Facchini, M.C., Fuzzi, S., Gobbi, G.P., Maione, M., Marinoni, A., Petzold, A., Roccato, F., Roger, J.-C., Sellegri, K., Sprenger, M., Venzac, H., Verza, G.P., Villani, P., Vuillermoz, E., 2008. The ABC-Pyramid Atmospheric Research Observatory in Himalaya for aerosol, ozone and halocarbon measurements. Sci. Total. Environ. 391 (2–3), 252–261.

Bonasoni, P., Laj, P., Marinoni, A., Sprenger, M., Angelini, F., Arduini, J., Bonafè, U., Calzolari, F., Colombo, T., Decesari, S., Di Biagio, C., di Sarra, G., Duchi, R., Facchini, M.-C., Fuzzi, S., Gobbi, G.P., Maione, M., Panday, A., Roccato, F., Sellegri, K., Verza, G.-P., Venzac, H., Villani, P., Vuillermoz, E., Cristofanelli, P., 2010. Atmospheric brown clouds in the Himalayas: first two years of continuous observations at the Nepal-Climate Observatory at Pyramid (5079 m). Atmos. Chem. Phys. 10 (15), 7515–7531.

Bond, T.C., Anderson, T.L., Campbell, D., 1999. Calibration and intercomparison of filter-based measurements of visible light absorption by aerosols. Aerosol Sci. Tech. 30, 582–600.

Carrico, C.M., Kus, P., Rood, M.J., Quinn, P.K., Bates, T.S., 2003. Mixtures of pollution, dust, sea salt, and volcanic aerosol during ACE-Asia: radiative properties as a function of relative humidity. J. Geophys. Res. 108. doi:10.1029/2003JD003405.

Chi, K.H., Lin, C.-Y., Yang, C.-F., Wang, J.-L., Lin, N.-H., Sheu, G.-R., Lee, C.-T., 2010. PCDD/F measurement at a high-altitude station in central Taiwan:

Author's personal copy

evaluation of long-range transport of PCDD/Fs during the southeast Asia biomass burning event. Environ. Sci. Technol. 44, 2954–2960.
Colette, A., Menut, L., Haeffelin, M., Morille, Y., 2008. Impact of the transport of aerosols from the free troposphere towards the boundary layer on the air quality in the Paris area. Atmos. Environ. 42, 390–402.
Collaud Coen, M., Weingartner, E., Schaub, D., Hueglin, C., Corrigan, C., Henning, S., Schwikowski, M., Baltensperger, U., 2004. Saharan dust events at the Jungfraujoch: detection by wavelength dependence of the single scattering albedo and first climatology analysis. Atmos. Chem. Phys. 4, 2465–2480.
Collaud Coen, M., Weingartner, E., Nyeki, S., Cozic, J., Henning, S., Verheggen, B., Gehrig, R., Baltensperger, U., 2007. Long-term trend analysis of aerosol variables at the high-alpine site Jungfraujoch. J. Geophys. Res. 112, D13213. doi:10.1029/2006JD007995.
Collaud Coen, M., Weingartner, E., Apituley, A., Ceburnis, D., Fierz-Schmidhauser, R., Flentje, H., Henzing, J.S., Jennings, S.G., Moerman, M., Petzold, A., Schmid, O., Baltensperger, U., 2010. Minimizing light absorption measurement artifacts of the Aethalometer: evaluation of five correction algorithms. Atmos. Meas. Tech. 3, 457–474. doi:10.5194/amt-3-457-2010.
Collaud Coen, M., Weingartner, E., Furger, M., Nyeki, S., Prévôt, A.S.H., Steinbacher, M., Baltensperger, U., 2011. Aerosol climatology and planetary boundary influence at the Jungfraujoch analyzed by synoptic weather types. Atmos. Chem. Phys. 11, 5931–5944.
Cristofanelli, P., Marinoni, A., Arduini, J., Bonafe, U., Calzolari, F., Colombo, T., Decesari, S., Duchi, R., Facchini, M.C., Fierli, F., Finessi, E., Maione, M., Chiari, M., Calzolai, G., Messina, P., Orlandi, E., Roccato, F., Bonasoni, P., 2009. Significant variations of trace gas composition and aerosol properties at Mt. Cimone during air mass transport from North Africa — contributions from wildfire emissions and mineral dust. Atmos. Chem. Phys. 9, 4603–4619.
Cristofanelli, P., Bracci, A., Sprenger, M., Marinoni, A., Bonafè, U., Calzolari, F., Duchi, R., Laj, P., Pichon, J.M., Roccato, R., Venzac, H., Vuillermoz, E., Bonasoni, P., 2010. Tropospheric ozone variations at the Nepal Climate Observatory-Pyramid (Himalayas, 5079 m a.s.l.) and influence of deep stratospheric intrusion events. Atmos. Chem. Phys. 10, 6537–6549.
De Tomasi, F., Tafuro, A.M., Perrone, M.R., 2006. Height and seasonal dependence of aerosol optical properties over southeast Italy. J. Geophys. Res. 111, D10203. doi:10.1029/2005JD006779.
Delene, D.J., Ogren, J.A., 2002. Variability of aerosol optical properties at four North American surface monitoring sites. J. Atmos. Sci. 59, 1135–1150.
Diaz, A.M., Diaz, J.P., Exposito, F.J., Hernandez-Leal, P.A., Savoie, D., Querol, X., 2006. Air masses and aerosols chemical components in the free troposphere at the subtropical northeast Atlantic region. J. Atmos. Chem. 53, 63–90.
Doherty, S.J., Quinn, P.K., Jefferson, A., Carrico, C.M., Anderson, T.L., Hegg, D., 2005. A comparison and summary of aerosol optical properties as observed in situ from aircraft, ship, and land during ACE-Asia. J. Geophys. Res. 110, D04201. doi:10.1029/2004JD004964.
Dubovik, O., Holben, B., Eck, T.F., Smirnov, A., Kaufman, Y.J., King, M.D., Tanré, D., Slutsker, I., 2002. Variability of absorption and optical properties of key aerosol types observed in worldwide locations. J. Atmos. Sci. 59, 590–608. doi:10.1175/1520-0469.
Eck, T.F., Holben, B.N., Reid, J.S., Dubovik, O., Smirnov, A., O'Neil, N.T., Slutsker, I., Kinne, S., 1999. Wavelength dependence of the optical depth of biomass burning, urban, and desert dust aerosols. J. Geophys. Res. 104 (D24), 31,333–31,349.
Fierz-Schmidhauser, R., Zieger, P., Gysel, M., Kammermann, L., DeCarlo, P.F., Baltensperger, U., Weingartner, E., 2010. Measured and predicted aerosol light scattering enhancement factors at the high alpine site Jungfraujoch. Atmos. Chem. Phys 10, 2319–2333.
Fischer, H., Kormann, R., Klüpfel, T., Gurk, C., Königstedt, R., Parchatka, U., Mühle, J., Rhee, T.S., Brenninkmeijer, C.A.M., Bonasoni, P., Stohl, A., 2003. Ozone production and trace gas correlations during the June 2000 MINATROC intensive measurement campaign at Mt. Cimone. Atmos. Chem. Phys. 3, 725–738.
Fischer, E.V., Jaffe, D.A., Marley, N.A., Gaffney, J.S., Marchany-Rivera, A., 2010. Optical properties of aged Asian aerosols observed over the U.S. Pacific Northwest. J. Geophys. Res. 115 (D20209). doi:10.1029/2010JD013943.
Gallagher, J.P., McKendry, I.G., Macdonald, A.M., Leaitch, W.R., 2011. Seasonal and diurnal variations in aerosol concentration on Whistler Mountain: boundary layer influence and synoptic scale controls. J. Appl. Meteorol. Clim.. doi:10.1175/JAMC-D-11-028.1.
Gebhart, K.A., Copeland, S., Malm, W.C., 2001. Diurnal and seasonal patterns in light scattering, extinction, and relative humidity. Atmos. Environ. 35, 5177–5191.
Hampl, V., Kerker, M., Cooke, D.D., Matijevic, E., 1971. Scavenging of aerosol particles by a falling water droplet. J. Atmos. Sci. 28, 1211–1221.
Haywood, J.M., Ramaswamy, V., 1998. Global sensitivity studies of the direct radiative forcing due to anthropogenic sulfate and black carbon aerosols. J. Geophys. Res. 103, 6043–6058.
Haywood, J.M., Shine, K.P., 1995. The effectof anthropogenic sulfate and soot aerosol on the clear sky planetary radiation budget. Geophys. Res. Lett. 22, 603–606.
Hegg, D., Hobbs, P.V., 1983. Preliminary measurements on the scavenging of sulfate and nitrate by clouds. Precipitation, Scavenging. : Dry Deposition and Resuspension, Vol. I. Elsevier Science, pp. 78–89.
Hitzenberger, R., Ctyroky, P., Berner, A., Tursic, J., Podkrajsek, B., Grgic, I., 2006. Size distribution of black (rBC) and total carbon in Vienna and Ljubljana. Chemosphere 65, 2106–2113.
Kent, G.S., Trepte, C.R., Lucker, P.L., 1998. Long-term Stratospheric Aerosol and Gas Experiment I and II measurements of upper tropospheric aerosol extinction. J. Geophys. Res. 103, 28,863–28,874.
Kivekas, N., Sun, J., Zhan, M., Kerminen, V.-M., Hyvarinen, A., Komppula, M., Viisanen, Y., Hong, N., Zhang, Y., Kulmala, M., Zhang, X.-C., Deli-Geer, Lihavainen, H., 2009. Long term particle size distribution measurements at Mount Waliguan, a high-altitude site in inland China. Atmos. Chem. Phys. 9, 5461–5474.
Kleissl, J., Honrath, R.E., Dziobak, M.P., Tanner, D., valMartin, M., Owen, R.C., Helmig, D., 2007. Occurrence of upslope flows at the Pico mountaintop observatory: a case study of orographic flows on a small, volcanic island. J. Geophys. Res. 112. doi:10.1029/2006JD007565.
Laj, P., et al., 2009. Measuring atmospheric composition change. Atmos. Environ. 43, 5351–5414.
Leaitch, W.R., Macdonald, A.M., Anlauf, K.G., Liu, P.S.K., Toom-Sauntry, D., Li, S.-M., Liggio, J., Hayden, K., Wasey, M.A., Russell, L.M., Takahama, S., Liu, S., van Donkelaar, A., Duck, T., Martin, R.V., Zhang, Q., Sun, Y., McKendry, I., Cubison, M., 2009. Evidence for Asian dust effects from aerosol plume measurements during INTEX-B 2006 near Whistler, BC. Atmos. Chem. Phys. 9, 3523–3546.
Lin, Y.C., Lin, C.Y., Hsu, W.T., 2010. Observations of carbon monoxide mixing ratios at a mountain site in central Taiwan during the Asian biomass burning season. Atmos. Res. 95, 270–278.
Liu, H., Pinker, R.T., Chin, M., Holben, B., Remer, L., 2008a. Synthesis of information on aerosol optical properties. J. Geophys. Res. 113 (D07206). doi:10.1029/2007JD008735.
Liu, D., Wang, Z., Liu, Z., Winker, D., Trepte, C., 2008b. A height resolved global view of dust aerosols from the first year CALIPSO lidar measurements. J. Geophys. Res. 113 (D16214). doi:10.1029/2007JD009776.
Lugauer, M., Baltensperger, U., Furger, M., Gaggeler, H.W., Jost, D.T., Schwikowski, M., Wanner, H., 1998. Aerosol transport to the high Alpine sites Jungfraujoch (3454 m asl) and Colle Gnifetti (4452 m asl). Tellus (B) 50, 76–92.
Macdonald, A.M., Anlauf, K.G., Leaitch, W.R., Chan, E., 2011. Interannual variability of ozone and carbon monoxide at the Whistler high elevation site: 2002–2006. Atmos. Chem. Phys. Discuss. 11, 1–44. doi:10.5194/acpd-11-1-2011.
Marcq, S., Laj, P., Roger, J.C., Villani, P., Sellegri, P., Bonasoni, P., Marinoni, A., Cristofanelli, P., Verza, G.P., Bergin, M., 2010. Aerosol optical properties and radiative forcing in the high Himalaya based on measurements at the Nepal Climate Observatory—Pyramid site (5079 m a.s.l.). Atmos. Chem. Phys. 10 (13), 5859–5872.
Maring, H., Savoie, D.L., Izaguirre, M.A., McCormick, C., Arimoto, R., Prospero, J.M., Pilinis, C., 2000. Aerosol physical and optical properties and their relationship to aerosol composition in the free troposphere at Izana, Tenerife, Canary Islands, during July 1995. J. Geophys. Res. 105, 14,677–14,700.
Marinoni, A., Cristofanelli, P., Calzolari, F., Roccato, F., Bonafe, U., Bonasoni, P., 2008. Continuous measurements of aerosol physical parameters at the Mt. Cimone GAW station (2165 m a.s.l., Italy). Sci. Total. Environ. 391 (2–3), 241–251.
Marinoni, A., Cristofanelli, P., Duchi, R., Calzolai, F., Decesari, S., Sellegri, K., Laj, P., Vuillermoz, E., Verza, G.P., Bonasoni, P., 2010. Aerosol mass and black carbon concentrations, two year-round observations at NCO-P (5079 m, Southern Himalayas). Atmos. Chem. Phys. 10 (17), 8551–8562.
Matthias, V., Balis, D., Bösenberg, J., Eixmann, R., Iarlori, M., Komguem, L., Mattis, I., Papayannis, A., Pappalardo, G., Perrone, M.R., Wang, X., 2004. Vertical aerosol distribution over Europe: statistical analysis of Raman lidar data from 10 European Aerosol Research Lidar Network (EARLINET) stations. J. Geophys. Res. 109, D18201. doi:10.1029/2004JD004638.
Mattis, I., Ansmann, A., Muller, D., Wandinger, U., Althausen, D., 2004. Multiyear aerosol observations with dual wavelength Raman lidar in the framework of EARLINET. J. Geophys. Res. 109. doi:10.1029/2004JD004600.
Mattis, I., Muller, D., Ansmann, A., Wandinger, U., Preißler, J., Seifert, P., Tesche, M., 2008. Ten years of multiwavelength Raman lidar observations of free-tropospheric aerosol layers over central Europe: geometrical properties and annual cycle. J. Geophys. Res. 113, D20202. doi:10.1029/2007JD009636.
McKendry, I.G., Hacker, J.P., Stull, R., Sakiyama, S., Mignacca, D., Reid, K., 2001. Long-range transport of Asian dust to the Lower Fraser Valley, British Columbia, Canada. J. Geophys. Res. 106, 18,361–18,370.
McKendry, I.G., Strawbridge, K.B., O'Neill, N.T., Macdonald, A.M., Liu, P.S. K., Leaitch, W.R., Anlauf, K.G., Jaegle, L., Fairlie, T.D., Westphal, D.L.,

Author's personal copy

2007. Trans-Pacific transport of Saharan dust to western North America: a case study. J. Geophys. Res. 112, D01103. doi:10.1029/2006JD007129.
McKendry, I.G., Gallagher, J., Campuzano Jost, P., Bertram, A., Strawbridge, K., Leaitch, R., Macdonald, A.M., 2010. Ground-based remote sensing of an elevated forest fire aerosol layer at Whistler, BC: implications for interpretation of mountaintop chemistry. Atmos. Chem. Phys. 10, 11,921–11,930.
McKendry, I.G., Strawbridge, K., Karumudi, M.L., O'Neill, N., Macdonald, A.M., Leaitch, R., Jaffe, D., Cottle, P., Sharma, S., Sheridan, P., Ogren, J., 2011. Californian forest fire plumes over Southwestern British Columbia: lidar, sunphotometry, and mountaintop chemistry observations. Atmos. Chem. Phys. 11, 465–477.
Mendonca, B.G., 1969. Local wind circulation on the slope of Mauna Loa. J. Appl. Meteorol. 8, 533–541.
Müller, T., Nowak, A., Weidensohler, A., Sheridan, P., Laborde, M., Covert, D.S., Marinoni, A., Imre, K., Henzing, B., Roger, J.-C., Martins dos Santos, S., Wilhelm, R., Wang, Y.-Q., de Leeuw, G., 2009. Angular illumination and truncation of three different integrating nephelometers: implications for empirical size-based corrections. Aerosol Sci. Technol. 43, 581–586.
Müller, T., Henzing, J.S., de Leeuw, G., Wiedensohler, A., Alastuey, A., Angelov, H., Bizjak, M., Collaud Coen, M., Engström, J.E., Gruening, C., Hillamo, R., Hoffer, A., Imre, K., Ivanow, P., Jennings, G., Sun, J.Y., Kalivitis, N., Karlsson, H., Komppula, M., Laj, P., Li, S.-M., Lunder, C., Marinoni, A., Martins dos Santos, S., Moerman, M., Nowak, A., Ogren, J.A., Petzold, A., Pichon, J.M., Rodriquez, S., Sharma, S., Sheridan, P.J., Teinilä, K., Tuch, T., Viana, M., Virkkula, A., Weingartner, E., Wilhelm, R., Wang, Y.Q., 2011. Characterization and intercomparison of aerosol absorption photometers: result of two intercomparison workshops. Atmos. Meas. Tech. 4, 245–268.
Nessler, R., Weingartner, E., Baltensperger, U., 2005. Adaptation of dry nephelometer measurements to ambient conditions at the Jungfraujoch. Environ. Sci. Technol. 39 (7), 2219–2228.
Nojarov, P., Ivanov, P., Kalapov, I., Penev, I., Drenska, M., 2009. Connection between ozone concentration and atmospheric circulation at peak Moussala. Theor. Appl. Climatol. 98, 201–208.
Nyeki, S., Baltensperger, U., Colbeck, I., Jost, D.T., Weingartner, E., Gaggeler, H.W., 1998a. The Jungfraujoch high-alpine research station (3454 m) as a background clean continental site for the measurement of aerosol parameters. J. Geophys. Res. 103, 6097–6107.
Nyeki, S., Li, F., Weingartner, E., Streit, N., Colbeck, I., Gäggeler, H.W., Baltensperger, U., 1998b. The background aerosol size distribution in the free troposphere: an analysis of the annual cycle at a high-alpine site. J. Geophys. Res. 103 (D24), 31,749–31,761.
Ogren, J.A., 2010. Comment on "Calibration and intercomparison of filter-based measurements of visible light absorption by aerosols". Aerosol Sci. Technol. 44, 589–591.
Perry, K.D., Cahill, T.A., Schnell, R.C., Harris, J.M., 1999. Long-range transport of anthropogenic aerosols to the National Oceanic and Atmospheric Administration baseline station at Mauna Loa Observatory, Hawaii. J. Geophys. Res. 104, 18,521–18,533.
Petzold, A., Schloesser, H., Sheridan, P.J., Arnott, W.P., Ogren, J.A., Virkkula, A., 2005. Evaluation of multiangle absorption photometry for measuring aerosol light absorption. Aerosol Sci. Technol. 39, 40–51.
Putaud, J.P., Raes, F., van Dingenen, R., et al., 2004. European aerosol phenomenology — 2: chemical characteristics of particulate matter at kerbside, urban, rural and background sites in Europe. Atmos. Environ. 38, 2579–2595.
Raes, F., Van Dingenen, R., Cuevas, E., Van Velthoven, F.J.V., Prospero, J.M., 1997. Observations of aerosol in the free troposphere and marine boundary layer of the subtropical northeast Atlantic: discussion of processes determining their size distribution. J. Geophys. Res. 102, 21,315–21,328.
Reid, J.S., Eck, T.F., Christopher, S.A., Hobbs, P.V., Holben, B., 1999. Use of the Angstrom exponent to estimate the variability of optical and physical properties of aging smoke particles in Brazil. J. Geophys. Res. 104 (D22), 27,473–27,489.
Reid, J.S., Eck, T.F., Christopher, S.A., Koppmann, R., Dubovik, O., Eleuterio, D.P., Holben, B.N., Reid, E.A., Zhang, J., 2005. A review of biomass burning emissions part III: intensive optical properties of biomass burning particles. Atmos. Chem. Phys. 5, 827–849.
Rodríguez, S., Alastuey, A., Alonso-Pérez, S., Querol, X., Cuevas, E., Abreu-Afonso, J., Viana, M., Pandolfi, M., de la Rosa, J., 2011. Transport of desert dust mixed with North African industrial pollutants in the subtropical Saharan Air Layer. Atmos. Chem. Phys. Discuss. 11, 8841–8892.
Rodríquez, S., Gonzalez, Y., Cuevas, E., Ramos, R., Romero, P.M., Abreu-Afonso, J., Redondas, A., 2009. Atmospheric nanoparticle observations in the low free troposphere during upward orographic flows at Izana Mountain Observatory. Atmos. Chem. Phys. 9, 6319–6335.
Sanroma, E., Palle, E., Sanchez-Lorenzo, A., 2010. Long-term changes in insolation and temperatures at different altitudes. Environ. Res. Lett. 5.
Sellegri, K., Laj, P., Dupuy, R., Legrand, M., Preunkert, S., Putaud, J.-P., 2003. Size-dependent scavenging efficiencies of multicomponent atmospheric aerosols in clouds. J. Geophys. Res. 108 (D11). doi:10.1029/2002JD002749.
Shaw, G.E., 2007. Aerosols at a mountaintop observatory in Arizona. J. Geophys. Res. 112. doi:10.1029/2005JD006893.
Sheridan, P.J., Ogren, J.A., 1999. Observations of the vertical and regional variability of aerosol optical properties over central and eastern North America. J. Geophys. Res. 104, 16,793–16,805.
Sheridan, P.J., Delene, D.J., Ogren, J.A., 2001. Four years of continuous surface aerosol measurements from the Department of Energy's Atmospheric Radiation Measurement Program Southern Great Plains Cloud and Radiation Testbed site. J. Geophys. Res. 106 (20), 20,735–20,747.
Sheu, G.-R., Lin, N.-H., Wang, J.-L., Lee, C.-T., Yang, C.-F.O., Wang, S.-H., 2010. Temporal distribution and potential sources of atmospheric mercury measured at a high-elevation background station in Taiwan. Atmos. Environ. 44, 2393–2400.
Takahama, S., Schwartz, R.E., Russell, L.M., Macdonald, A.M., Sharma, S., Leaitch, W.R., 2011. Organic functional groups in aerosol particles from burning and non-burning forest emissions at a high-elevation mountain site. Atmos. Chem. Phys. 11, 6367–6386.
Targino, A.C., Noone, K.J., Ostrom, E., 2005. Airborne in-situ characterization of dry aerosol optical properties in a multisource influenced marine region. Tellus 57B, 247–260.
Toledano, C., Cachorro, V.E., Berjon, A., de Frutos, A.M., Sorribas, M., de la Morenab, B.A., Goloub, P., 2007. Aerosol optical depth and Ångström exponent climatology at El Arenosillo AERONET site (Huelva, Spain). Q. J. R. Meteorol. Soc. 133, 795–807.
Treffeisen, R.E., Thomason, L.W., Strom, J., Herber, A.B., Burton, S.P., Yamanouchi, T., 2006. Stratospheric Aerosol and Gas Experiment (SAGE) II and III aerosol extinction measurements in the Arctic middle and upper troposphere. J. Geophys. Res. 111, D17203. doi:10.1029/2005JD006271.
Turner, D.D., Ferrare, R.A., Brasseur, L.A., 2001. Average aerosol extinction and water vapor profiles over the Southern Great Plains. Geophys. Res. Lett. 28, 4441–4444.
van der Hulst, H.C., 1957. Light Scattering by Small Particles. John Wiley. 470 pp.
van Donkelaar, A., Martin, R.V., Brauer, M., Kahn, R., Levy, R., Verduzco, C., Villanueve, P.J., 2010. Global estimates of ambient fine particulate matter concentrations from satellite-based aerosol optical depth: development and application. Environ. Health Perspect. 118, 847–855.
Venzac, H., Sellegri, K., Laj, P., Villani, P., Bonasoni, P., Marinoni, A., Cristofanelli, P., Calzolari, F., Fuzzi, S., Decesari, S., Facchini, C., Vuillermoz, E., Verza, G.P., 2008. High frequency new particle formation in the Himalayas. Proc. Nat. Acad. Sci. 105 (41), 15,666–15,671.
Venzac, H., Sellegri, K., Villani, P., Picard, D., Laj, P., 2009. Seasonal variation of aerosol size distributions in the free troposphere and residual layer at the puy de Dôme station, France. Atmos. Chem. Phys. 9, 1465–1478.
Viana, M., Querol, X., Alastuey, A., Cuevas, E., Rodríguez, S., 2002. Influence of African dust on the levels of atmospheric particulates in the Canary Islands air quality network. Atmos. Environ. 36, 5861–5875.
Virkkula, A., Ahlquist, N.C., Covert, D.S., Arnott, W.P., Sheridan, P.J., Quinn, P.K., Coffman, D.J., 2005. Modification, calibration and a field test of an instrument for measuring light absorption by particles. Aerosol Sci. Technol. 39, 68–83.
Wandinger, U., et al., 2002. Optical and microphysical characterization of biomass-burning and industrial-pollution aerosols from multiwavelength lidar and aircraft measurements. J. Geophys. Res. 107 (D21), 8125. doi:10.1029/2000JD000202.
Wang, T., Wong, H.L.A., Tang, J., Ding, A., Wu, W.S., Zhang, X.C., 2006. On the origin of surface ozone and reactive nitrogen observed at a remote mountain site in the northeastern Qinghai-Tibetan Plateau, western China. J. Geophys. Res. 111 (D08303). doi:10.1029/2005JD006527.
Weingartner, E., Nyeki, S., Baltensperger, U., 1999. Seasonal and diurnal variation of aerosol size distributions ($10<d<750$ nm) at a high alpine site (Jungfraujoch 3580 m asl). J. Geophys. Res. 104, 26,809–26,820.
Weingartner, E., Saathoff, H., Schnaiter, M., Streit, N., Bitnar, B., Baltensperger, U., 2003. Absorption of light by soot particles: determination of the absorption coefficient by means of aethalometers. Aerosol Sci. 34, 1445–1463.
Weiss-Penzias, P., Jaffe, D., Swartzendruber, P., Dennison, J.B., Chand, D., Hafner, W., Prestbo, E., 2006. Observations of Asian air pollution in the free troposphere at Mount Bachelor Observatory during spring of 2004. J. Geophys. Res. 111. doi:10.1029/2005JD006522.
Weiss-Penzias, P., Jaffe, D., Swartzendruber, P., Hafner, W., Chand, D., Prestbo, E., 2007. Quantifying atmospheric mercury emissions from biomass burning and East Asian industrial regions based on ratios with carbon monoxide in pollution plumes at the Mount Bachelor Observatory. Atmos. Environ. 41, 4366–4379.

Author's personal copy

Winker, D.M., Hunt, W.H., McGill, M.J., 2007. Initial performance assessment of CALIOP. Geophys. Res. Lett. 34. doi:10:1029/2007GL030135.

Yu, H., Chin, M., Winker, D.M., Omar, A.H., Liu, Z., Kittaka, C., Diehl, T., 2010. Global view of aerosol vertical distributions from CALIPSO lidar measurements and GOCART simulations: regional and seasonal variations. J. Geophys. Res. 115. doi:10.1029/20090JD013364.

Zarzycki, C.M., Bond, T.C., 2010. How much can the vertical distribution of black carbon affect its global direct radiative forcing? Geophys. Res. Lett. 37, L20807. doi:10.1029/2010GL044555.

Zhou, L.X., Tang, J., Wen, Y., Yan, P., Zhang, X.-C., 2003. The impact of local wind and long-range transport on the continuous carbon dioxide record at Mount Waliguan, China. Tellus 55B, 145–158.